

THE UNIVERSITY OF MELBOURNE

Electrochemical tuning of a diamond voltage sensor

Author

Charlie PATTINSON

Under the Supervision of

Dr. David SIMPSON

Dr. Daniel MCCLOSKEY

Dr. Nikolai DONTSCHUK

Dr. Liam HALL

Presented in partial fulfillment of the requirements of the degree of Master of Science.

June 17, 2022

Abstract

Voltage sensing is paramount in the field of biology for understanding how networks of cells coordinate activity for the purpose of moving muscles or developing complex thought. Current technologies are reaching their theoretical limitations, and therefore new methods for voltage sensing are required to break new ground. The solution is a diamond voltage sensor. Nitrogen vacancy centres within diamond provide a novel optical indicator of voltage differences in solution but prior, to this work, have not been able to reach biologically relevant voltages and timescales. The work here proposes an electrochemical method to improve the diamond voltage sensor's sensitivity, attaining levels required for biological measurement.

The diamond voltage sensor uses the fluorescence of nitrogen vacancy centres to report on variations in the local electrical environment. The local electrical environment modifies a nitrogen vacancy's electronic configuration between three possible states, a positively(NV^+), neutrally(NV^0) and negatively(NV^-) charged state. We can measure these charge states of a nitrogen vacancy by their unique fluorescent profiles. As such by recording the nitrogen vacancy fluorescence, we can determine their state and therefore their electrical environment. Yet, there is significant work required before reaching biologically relevant voltages and time-scales.

This thesis makes significant progress for diamond voltage sensing technologies by reporting a 20 times improvement in the voltage sensitivity compared to existing attempts in the literature. By electrochemically tuning the surface of the diamond in solution, it was shown that the diamond voltage sensor can be oxidized to reach an optimal level for sensing. In fact, sensitivities of the diamond voltage sensor were improved by more than a factor of 30 when comparing the states prior and post tuning. These results were reported for a sensor detecting transitions between the NV^0 and NV^+ states using their fluorescence or non-fluorescence respectively. A similar optimisation procedure was used to explore an alternate sensing modality characterised by transitions between the two more electronegative nitrogen vacancy charge states, NV^0 and NV^- . The alternate sensing modality is a dual charge state sensor as it provides two simultaneous signals to report on the electrical environment. Following this, a characterisation of the nitrogen vacancy charge state populations was undertaken by using a machine learning algorithm to decompose the fluorescence and led to estimations of the optimal charge state populations for the dual charge state sensing modality.

This work paves the way for realising a diamond voltage sensor as a strong competitor in the market of voltage imaging technologies. Furthermore, the techniques pioneered here lay the ground work for a new voltage sensor capable of recording at resolutions and voltage sensitivities not possible with current technologies.

Acknowledgments

I would first of all like to thank my supervisors David Simpson and Liam Hall for their support and guidance throughout this journey. They continually believed in me and my abilities, and helped me to develop a strong confidence in the subject matter as demonstrated by this thesis. I owe a world of thanks to Daniel McCloskey and Nikolai Dotschuk for the work they did in preparing samples and providing ongoing advice on the work done in this thesis. Not to mention their elucidating answers to many of my physics related questions, project-specific or not, which always serve to remind me why I love physics. I would like to thank the entire quantum sensing group, Hunter Johnson, Ella Walsh, Sam Scholten, and many more for their feedback throughout this process and sharing in all the highs and lows of the project with me.

My friends, Oscar and Liam, were inspirations for me to start my Masters of Science (Physics) and the discussions and learnings I have taken from them have been invaluable. Thank you for pushing me. Finally to my family, my mother Amanda and father Warwick thank you both for being an inspiration in academia and providing thoughtful feedback and encouragement throughout my journey. To all friends and family, thank you for listening to all my successes and failures throughout this thesis with an honest intrigue and interest in my work. You always helped me to look out for the many amazing components of this journey and be grateful for the opportunity to undertake and complete this piece of work.

Statement of contribution

This is to certify that the following thesis is 50 pages in length and is my own work unless otherwise specified. Chapter 1 lays out a clear motivation for a diamond voltage sensor and explains the important constituents for operation and future optimisation. Chapter 2 takes on an important element of optimisation for the diamond voltage sensor: the surface chemistry. The second chapter realises electrochemical methods for tuning the surface chemistry of diamond while simultaneously reporting on its capability as a voltage sensor. The results from the second chapter indeed show that an optimal state can be reached by electrochemical methods and can improve sensitivity by a factor of 30 from its initial state. Not only this, but the optimal contrast reached is an improvement by a factor of 20 over measurements currently reported in the literature. The results of this chapter contributed to a paper (McCloskey D.J, Dotschuk, N, Pattinson C. et al. *A Diamond Voltage Imaging Microscope* Nature Photonics (accepted) 13th June 2022). Finally, Chapter 3 provides an exploration into a secondary sensing modality predicated on the NV⁰ /NV⁻ transition. The secondary sensing modality would provide lower contrast but two anti-correlated signals that would support a greater robustness to noise. Significant work was made in understanding what appropriate NV⁰ and NV⁻ populations would be required. Not only this but an algorithm was developed to characterise features in a set of spectra, to report on the relative populations of NV states from spectral measurements, and evaluate sensors prior to tuning. The third chapter also outlines the results of a significant python code base developed by the author for building a decomposition algorithm for NV charge state fluorescence and interpreting the results in their context of a diamond voltage sensor. These results will continue to be used for characterisation of diamond voltage sensors in future. The work undertaken throughout this thesis also led to the development of several automated programs required to optimise and characterise the sensors in this work using camera, spectrometer and photodiode measurements concurrently.

List of abbreviations

Notation	Description	Page List
AFM	Atomic force microscopy	6
AOM	Acousto-optic modulator	17
BDD	Boron-doped diamond	2
CV	Cyclic voltammetry	6
CVD	Chemical vapour deposition	3
EA	Electron affinity	4
EBL	Electron beam lithography	15
EDL	Electrolytic double layer	16
EIS	Electrochemical impedance spectroscopy	6
HPHT	High pressure high temperature	3
LED	Light emitting diodes	7
MEA	Multi-electrode array	1
MPE-CVD	Microwave Plasma Enhanced Chemical Vapour deposition	15
ND	Nanodiamond	10
NEA	Negative electron affinity	4
NMF	Non-negative matrix factorization	36
NV	Nitrogen vacancy	2
NV ⁺	Positively charged nitrogen vacancy	3
NV ⁻	Negatively charged nitrogen vacancy	3
NV ⁰	Neutral nitrogen vacancy	3
ODMR	Optically detectable magnetic resonance	3
PEA	Positive electron affinity	4
VSD	Voltage sensitive dye	1
XPS	X-ray photoyield spectroscopy	5
ZPL	Zero phonon line	39

Contents

1 A diamond voltage sensor	1
1.1 A motivation	1
1.2 Diamond	2
1.3 Diamond doping	2
1.4 Surface oxidation	6
1.5 Band bending model	7
1.6 Sensing using near-surface NV centres	10
2 Electrochemical oxidation for tuning a diamond voltage sensor	15
2.1 Preparing the diamond voltage sensor	15
2.2 Electrochemically tuning the diamond	16
2.3 Recording Fluorescence	17
2.4 Diamond characterisation	18
2.5 The sensor optimisation	19
2.6 Conclusion and next steps	26
3 A deeper understanding with deeper NV centres	28
3.1 Methodology variations	28
3.2 The deeper implantation profile	32
3.3 The sensor optimisation	33
3.4 Distinguishing NV fluorescence using Non-Negative Matrix Factorization	36
4 Concluding remarks and next steps	43
Bibliography	45

Chapter 1

A diamond voltage sensor

1.1 A motivation

To understand our environment we need to measure it. Whether that is at the scales of the very small or the very large, devices with better resolution, precision and low measurement uncertainty are required to verify our present understanding of nature. Part of this endeavour is the art of measuring electrical activity. In 1780 Lucia and Luigi Galvani discovered that frogs' muscles twitched in response to electrical signals leading to the birth of the field of bioelectromagnetics. Their insight paved the way for understanding that electric signaling is the prime mechanism by which our body moves and thinks, and how our hearts beat. Between voltage measurement devices such as voltage sensitive dyes, multi-electrode arrays, and patch clamps, an understanding of electrical behaviour has been an active field over the past 50 years. However, as our knowledge of these complex biological systems has grown, we only find more questions to ask. One considerable question is how electrical signalling functions synthesise thoughts in our own brains.

In this endeavour to understand the field of voltage sensing in biological systems, two main sensors dominate: multi-electrode arrays and voltage sensitive dyes. Multi-electrode arrays (MEAs) consist of millions of electrical pins which measure electrical differences between their neighbouring pins to discern electrical activity. Voltage-sensitive dyes (VSDs) are molecules that can be introduced into biological systems and fluoresce depending on their electrical environment creating stunning imagery. However, they both have their shortcomings. MEAs are being limited by their density as a trade-off is reached: cross talk between pins degrades the measured signal and low-voltage measurements have to be compensated by large on-chip amplifiers. Voltage-sensitive dyes by contrast provide unparalleled resolution but are limited by photo-bleaching effects rendering them only reliable for short timescales.

A solution is to leverage the individual advantages of these technologies by introducing a diamond voltage sensor. The diamond voltage sensor uses the layout of an MEA and replaces the electrical pins with point-like optical defects that fluoresce, similar to a VSD, in response to electrical signals. There is no read out wires or bleached dyes, just repeatable electrical imaging that builds on the working principles of existing technologies. However, the diamond voltage sensor has not yet been realised as viable for biological sensing as it has not been able to reach relevant voltage sensitivities.

This thesis demonstrates that a careful tuning of the surface termination of the diamond can provide the required sensitivities for biological measurement. We apply an electrochemical method to vary the surface termination and report on the effects for single and dual charge state sensing candidates (corresponding to one or two fluorescence signals respectively). We explore this method by trialling different tuning techniques and different measures for recording their respective performance. Ultimately, we realise a sensor which exhibits a voltage sensitivity that is 20 times better than the current the state-of-the-art for single crystal diamond [1]. We also record the oxidation on a dual charge state sensing candidate and report on the required NV populations for dual charge state

sensors to be realised.

In this chapter, we first develop the constituents of this electrical sensor and discuss how surface chemistry changes can improve the sensitivity of the diamond voltage sensor. The following chapter develops the relevant ideas from condensed matter physics that are required to understand the diamond voltage sensor and its working mechanism. We will also discuss previous attempts of diamond voltage sensing and their limitations. Finally, we will define some key concepts and metrics which we will use throughout this thesis to evaluate the diamond voltage sensor's performance.

1.2 Diamond

Diamond has demonstrated itself as a quintessential material in the study of solid-state physics. It is a tough material due to its 4 tetrahedral carbon bonds which subsequently create a rigid structure and a stable environment for novel physical behaviour. The stability of these carbon bonds contributes to a chemical inertness of the diamond. This chemical inertness has attracted the attention of biomedical engineers for its biological compatibility, remaining non-toxic when in contact with organic specimens of interest. Diamond's crystalline structure also provides room for interesting electrical and optical behaviour. As a wide band gap semiconductor (5.5eV, [2]), diamond is transparent to visible light. Furthermore, the wide band gap provides ample room for alternate implanted electronic states. These implanted states can then facilitate transitions that exist in the visible spectrum. Diamond's lattice structure endows it with high thermal conductivity, promoting it as suitable for dissipating large amounts of heat from high powered electrical or optical sources; an attractive quality in the electronics industry. The key point we will focus on next is the manipulation of diamond by adding alternate chemical species to the diamond to the bulk or to the surface (doping). By doping the diamond we can begin to leverage a few of these favourable properties.

1.3 Diamond doping

Diamond can be doped both in its bulk as well as on its surface leading to changes in its electronic and optical characteristics. Here we will discuss both the bulk and surface doping and focus on their interplay for electrical sensing.

1.3.1 Bulk doping

Bulk doping can create optical defects in diamond or provide increased electrical conductivity. For diamond there exists several different defects which can be detected optically such as Nitrogen (yellow) or Boron (blue). Boron in particular has demonstrated itself as a useful p-type dopant giving rise to very low resistivities of $1\text{-}2 \Omega\cdot\text{cm}$ [3] compared to regular diamond with resistivities of $10^{16} \Omega\cdot\text{cm}$. Boron doped diamond (BDD) electrodes have demonstrated themselves as useful in many applications such as wastewater treatment [4], biomedical applications [5] or electronics [6].

Fluorescent defects in diamond can also take the form of complexes spanning multiple lattice sites. One key example is the Nitrogen-Vacancy (NV) centre. The NV centre consists of two defects adjacent to each other, a nitrogen atom and a vacant lattice site or vacancy. The NV centre will be the principal bulk defect that we will explore throughout this research and its fluorescent behaviour will be the primary mechanism first tuned, and later exploited for electrical sensing. Before this we will first discuss how these defects find their way into the diamond. The distribution of the NV centres throughout the diamond varies with the implantation method and acts as an independent variable for realising either a single or dual charge state diamond voltage sensor.

Bulk doping methods

Bulk doping can be experimentally achieved either in the process of growing the diamond [7] or by subjecting pure diamond to irradiation (most commonly in the case of ion implantation) [8]. Diamond can be found naturally with existing impurities, as an artifact of its environmental conditions, or it can be grown from a seed crystal using either chemical vapour deposition (CVD) or high-pressure high temperature (HPHT) techniques. HPHT techniques typically populate the diamond with many unwanted defects and are typically not desirable for sensing applications but for applications where the hardness of diamond is required (e.g diamond-encrusted drill bits). CVD diamond is much more common in the scientific community where diamond can be precisely doped with desired chemical species. The CVD method is very popular in semiconductor physics due to the ease with which thin films can be placed within a fabricated device.

Ion implantation is a common form of irradiation in which ions are fired at a sample at a specific angle and kinetic energy (measured in keV) to place them at a distribution of depths. The following investigation explores nitrogen implanted at two main implantation energies, 2keV and 4keV. These two implantation energies are crucial in the subsequent analysis as they place the dopants at different depths in the diamond. These different depths provide different electrical environments with dopants at shallow depths (in the 2keV case) more sensitive to changes in the external environment. For example when exposed to air, free electrons in the atmosphere will on average have a higher chemical potential than electrons within the diamond (as they are not bound). As a result there is a build up of negative ions on the surface of the diamond leading to more electro-positive dopant states to screen the negative charge. By comparison dopants further into the bulk can favour more electronegative states as the stand off to the surface charge is greater and the coulombic interaction weaker. The description laid here is more completely discussed in reference to the band bending diagrams addressed in [Section 1.5](#).

The Nitrogen-Vacancy (NV) centre is the defect of interest for this investigation. A two-part system that is shielded from the environment by the diamond's rigid structure has been used as a quantum sensor for magnetic [9], temperature, [10] and electrical imaging [11]. The NV centre can be categorised as one of many dopants that can be implanted in diamond and we now seek to understand it, and in particular its charge state structure.

1.3.2 Nitrogen Vacancy centre

The NV centre exists in three known charge states which each exhibit different possible fluorescence profiles. The three charge states consist of two that fluoresce, the negatively charged NV^- and the neutral NV^0 as well as a third *dark* state, the positively charged NV^+ . The NV^- charge state has been long established as an invaluable tool for quantum sensing due to its long spin coherence and effectiveness with optically detectable nuclear magnetic resonance (ODMR) [12]. However, to address the electrical activities of the environment the inter-conversion of these three different charge states becomes the mechanism of interest, not their spin characteristics. To distinguish between these different charge states we note their unique fluorescent profiles in [Figure 1.4.1](#). The NV^0 has a greater contribution in the wavelength range between 600nm to 700nm, whereas the NV^- spectrum has a greater contribution between wavelength of 650nm and 750nm. By contrast NV^+ is omitted here as it provides no measurable fluorescence in the wavelengths studied.

The equilibrium charge state concentration of the NV centres in the diamond can be altered by three main components: other neighbouring impurities [13], applied electric fields across the diamond [11, 1], and their proximity to the surface and the surface composition [14, 15, 11]. In this research, both electrical external fields and surface effects will be the principal mechanisms of interest; the former to sense and the latter to sensitise. Electrical sensing mechanisms have

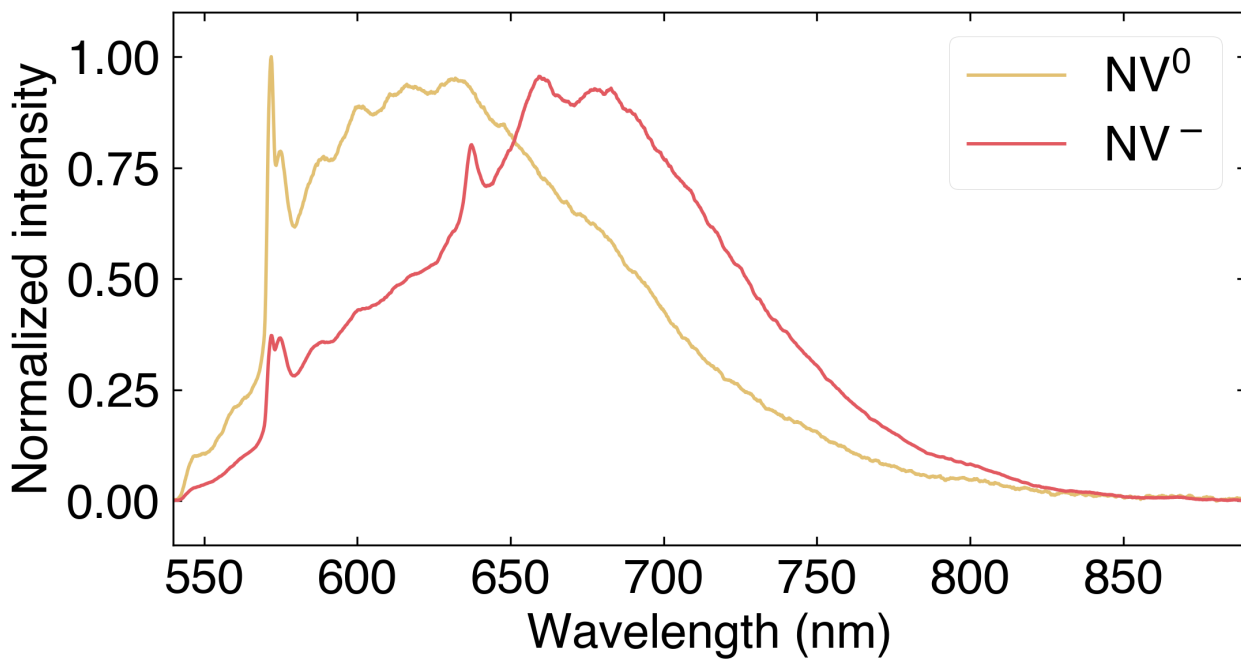


Figure 1.3.1: Approximate fluorescence profiles of the optically detectable NV charge states oxygen-terminated diamonds with strong NV^- concentrations and hydrogen-terminated diamonds with strong NV^0 populations.

already been experimentally explored in nanodiamonds [11] and bulk crystal [1]. In bulk diamond, the NV sensing sensitivity has even been suggested to be capable of detecting mammalian neurons through simulations [16]. However, the optimisation of the diamond voltage sensor as a recording device requires further development before reaching biological applications. One such development is to sensitise the device by modifying the surface termination so that changes in the environmental electric field are met readily with charge state transitions (e.g movement from NV^- to NV^0) in near-surface defects, this is known as surface transfer doping.

1.3.3 Surface transfer doping

Surface transfer doping, in contrast to bulk doping, is the modification of the surface of a material to change the electrical behaviour in the near-surface regime (on the order of 10nm). One of the primary metrics used in understanding doping characteristics, especially at surfaces, is the electron affinity. The electron affinity is a measure of the energetic tendency of a material to either gain (positive electron affinity, PEA) or lose (negative electron affinity, NEA) electrons and is measured as the energy exchanged (in eV).

In the study of diamond and its surface terminations, two main forms are most abundantly examined in the literature: oxygen termination and hydrogen termination. These two types of termination play a large role in the charge states of near-surface NV centres by changing the electron affinity (EA) at the surface of the diamond. The controlled conversion from hydrogen termination to oxygen termination (from an NEA to PEA respectively) will be the main exploration undertaken within this thesis. We will realise EAs at bespoke levels in between these extremes by electrochemically oxidising the surface.

Oxygen termination

Oxygen termination refers predominantly to the presence of hydroxyl groups (C-OH), ethers (C-O-C) and ketones (C=O) bonded to the surface of the diamond. The presence of these groups has

been demonstrated using X-ray photoelectron spectroscopy (XPS) [17], however, the exact densities of each oxygen species is still not well known. The densities of these oxygen species are believed to be dependent on the conditions under which the oxygen termination was created (e.g acid boil, oxygen plasma or vacuum ultraviolet ozone), the roughness of the surface and the temperature that the diamond is exposed to [18, 19]. It has been shown in theoretical calculations (using density functional theory) that the EA of hydroxyl groups are near-zero (0.03 eV) whereas ethers and ketones present a positive EA's of 2.61-4.66 eV and 3.64 eV respectively [20, 21]. The electron affinity of these oxygen species, however, has not been able to be verified experimentally for each species individually. Only bulk measurements of oxygen terminated diamond EA's have been realised. The experimental results provide an EA of 1.7eV, a suggested average of all the oxygen species present on the diamond [18]. The experimentally obtained value of 1.7eV will be referred to throughout the following investigation, however, there is still further work required to understand whether the tuning conducted in this thesis creates the presence of one of these oxygen species over another.

Hydrogen termination

Hydrogen termination of diamond was first discovered by Landstrass R. et al. [22] in 1989 with the advent of chemical vapour decomposition (CVD) to create diamond films. Hydrogen terminations came as a byproduct of the technique (synthesised with a methane and hydrogen gas) and demonstrated an unusually low electrical resistivity. More specifically, the hydrogen termination provided a sharp decrease in the surface resistivity of the diamond from 10^{16} to $10^6 \Omega \cdot \text{cm}$. It took a further 11 years before the properties that give rise to this conductivity were understood. The widely accepted model, developed by Maier et al. [23], was a surface transfer doping model which posited that hydrogen termination was required as well as exposure to air for the conductivity to present itself. It was proposed that a small water layer physisorbs to the surface of the diamond and is crucial for its conductivity. The surface transfer doping theory was bolstered by future work demonstrating that conductivity was greatly reduced in vacuum [24].

As shown by Riedel et al. [24] two key reactions take place. On the surface, a redox reaction occurs between the diamond and the water layer to provide p-type carriers (or holes), termed a 2-dimensional hole gas (2DHG). The diamond provides electrons to the physisorbed water layer and creating the holes within the diamond Eq. 1.3.1. The physisorbed water layer then provides any free H^+ ions to produce water and hydrogen gas as in Eq. 1.3.2.



The holes created by this surface transfer doping model then have two main mechanisms to respond to local electric field changes. Move within the surface in response to electrical fields or to react with the physisorbed layer moving between the two different sides of Eq. 1.3.1 and Eq. 1.3.2. The former is the predominant mechanism in sensing regimes.

Since the realisation of the favourable properties of hydrogen termination, alternate methods have also been developed to deposit hydrogen after the diamond growth. There are three notable techniques for creating hydrogen films on the surface of diamond remote microwave plasma [25], electrochemical techniques [26] or thermal hydrogenation [27]. The hydrogenation of diamond surfaces using a microwave plasma one of the techniques used for the samples studied in this thesis. The technique consists of providing molecular hydrogen to a chamber with the diamond at low pressures. Following the correct mixture in the chamber a plasma of hydrogen ions is created using high power microwave pulse and maintained. Hydrogenation is then facilitated as ions in the plasma deposit themselves on the diamond surface. However, the process has been known to etch diamond when attempting to terminate [25]. Electrochemical techniques for creating a hydrogen termination have

also been developed by Hoffman et al. in 2010 [26]. The technique by Hoffmann et al. exposes a boron-doped diamond to a hydrochloric acid solution and then applies an electrical current from the diamond to an electrode (cathode) in solution. This works to reduce hydrogen species onto the surface of the diamond creating the hydrogen surface layer. In this thesis we will seek to reverse this reaction oxidising the surface to regain an oxygen termination.

1.4 Surface oxidation

Surface oxidation is the process by which the surface of a material forms a layer, typically of an oxygen species, that is more energetically favourable than the original surface. The effect can be seen most readily in metals, for example with iron forming rust (iron oxide) over time with exposure to air and water. Oxidation is commonly also seen in other semiconductor materials, for example, silicon forming silicon dioxide in air at room temperature (in silicon's crystalline form). Carbon, belonging to the same group on the periodic table as silicon, also reacts with oxygen in its diamond form when exposed to atmosphere unless other surface terminations are already present. In fact, the oxidation of diamond may be one of the attributes that allowed the novel surface conductivity of hydrogen-terminated diamond to elude the scientific community until 1989.

In our case, the process of oxidation is an essential reaction that we will be electrically inducing on our diamond's surface. In solution, this process can be induced on a hydrogen-terminated surface by applying a sufficient voltage to surmount energetic barriers facilitating an exchange of surface ligands from hydrogen to oxygen species.

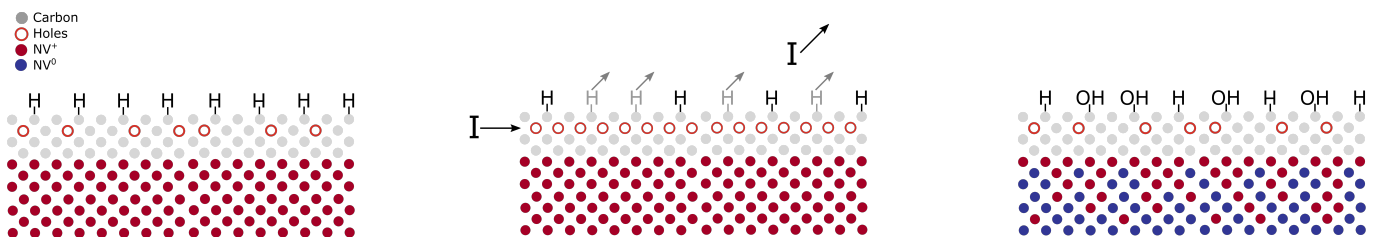
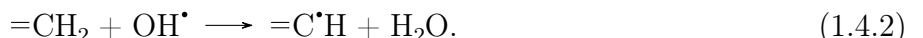


Figure 1.4.1: A schematic of how oxidation can be induced electrically in solution on the diamond surface. There is also the presence of other oxygen species but hydroxyl (-OH) groups have only been displayed for simplicity. The schematic also shows the decrease in 2DHG density and the change of the NV centres towards more electronegative charge states such as the NV⁰ state.

The electrochemical oxidation process has been employed by Hoffman et al. [28] on BDDs in a sulfuric and nitric acid solution over 10 samples. The 10 samples were exposed to voltages from 1-10V for 10 seconds. Afterwards, by using atomic force microscopy (AFM), x-ray photoelectron spectroscopy (XPS), as well as electrochemical impedance spectroscopy (EIS), they conclusively demonstrated that surface oxidation was achieved. Further work in understanding this oxidation effect has also been explored by Chaplin et al. [29] using cyclic voltammetry (CV). Cyclic voltammetry involves scanning through voltages (typically at a rate of 100mV.s⁻¹) and recording the corresponding currents. Cyclic voltammograms were recorded for 5 BDD electrodes subject to different oxidation current densities of 0, 5, 50 and 500 mA.cm⁻². Within this work a number of reactions were proposed as responsible for the removal of hydrogen species in Eq. 1.4.1 and Eq. 1.4.2,



The removal of hydrogen in these reactions are then followed by a replacement with oxygen species in Eq. 1.4.3 and Eq. 1.4.4,



Interestingly, these reactions suggest a dominant presence of OH^\bullet radicals. It is furthermore possible from here to also convert OH^\bullet radicals into ketones ($\text{C}=\text{O}$) when provided sufficient voltages (greater than 1.74 V). The peaks in cyclic voltammograms also provide estimations of the activation voltages for the oxidative process. The peaks represent higher than expected currents for specific voltages and therefore a lower total resistance due to the creation of a new parallel electrical pathway. This new electrical pathway is typically a chemical reaction made available only at certain voltages or activation energies. The use of voltage versus current helps to better elucidate different electrical characteristics of the diamond and will also be explored further in later chapters.

Even though the surface oxidation by Hoffman et al. was successful the voltages applied were derived empirically and caused large changes in the fraction of hydrogen-terminated diamond that was oxidised [28]. The oxidation undertaken by Hoffman et al. was also executed in an acidic solution which may lessen the rate of oxidation (due to less OH^\bullet radicals in solution). Throughout this thesis, experimenting with different oxidation voltages was made difficult due to inconsistencies between fabrication methods, and thus the threshold for oxidation was often derived on a per device basis.

We will seek to replicate the work done by Hoffman et al. with three key differences. First, we will use near-surface NV centres as an indicator for understanding the surface chemistry. By implementing a non-destructive and *in situ* recording of the NV fluorescence, we can quickly and continuously measure the surface changes on a single chip throughout smaller oxidation steps. Second, we will avoid using boron-doped diamond and require the current to flow through the conductive hydrogen surface. We require the diamond to be resistive in its bulk for the NV centres to operate effectively as a sensor. Third, we will conduct the oxidation in phosphate buffered saline (PBS) to reduce any wear to the components of the sensor and to sensitize the chip in conditions commensurate with biological recordings. By using phosphate buffered saline with a pH of ≈ 7.4 the oxidation may also require lower voltages, and may reach a further oxidised state.

We have now developed a firm understanding of the relevant constituents of the diamond voltage sensor as well as contextual literature. To combine all these constituents and display their interplay, it is useful to consider a graphical representation which is commonplace in semiconductor physics: the band bending model.

1.5 Band bending model

The band bending model provides an important graphical insight into semiconductor behaviour and in particular how materials interact at interfaces. The band diagram explores the energetic behaviour of free (conduction) electrons compared to bound (valence) electrons in materials. The most commonplace comparison is in comparing the energy diagrams of insulators, semiconductors and conductors in Figure 1.5.1.

Within the context of semiconductor materials, the band diagram aids in understanding the zone that is in between conduction and valence states: the bandgap. For a pure semiconductor material, the bandgap is a forbidden zone meaning that to move from a bound state to a free state, an electron must absorb energy greater than or equal to the bandgap. The technology of LEDs relies on this phenomenon for its operation as electrons traverse this bandgap from the conduction band to the valence band and emit photons to provide visible light. In the case of diamond, this

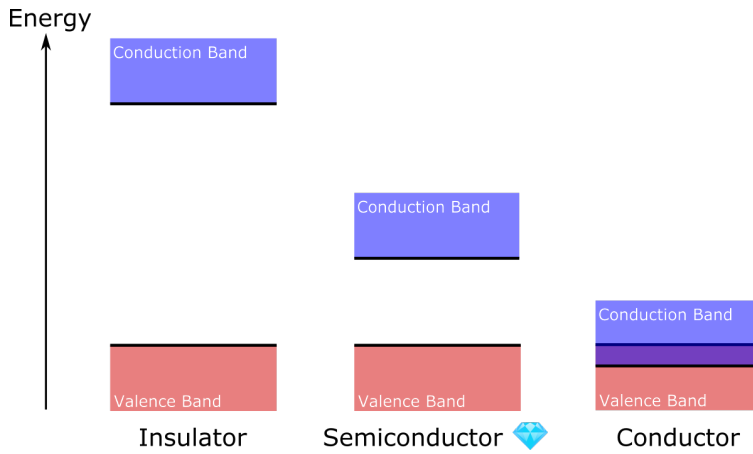


Figure 1.5.1: A comparison between the band diagrams of insulators, semiconductors (such as diamond) and conductors.

band gap is wider than other materials such as silicon or germanium (5.5eV compared to 1.17eV and 0.74eV respectively [2]) and thus earns its name as a wide bandgap semiconductor. The large bandgap makes it too wide for electrons traversing it to be absorbing/emitting photons in the visible spectrum leading to its optical transparency. The bandgap also allows for defects such as the NV centre to sit, energetically, within it. Furthermore, the width of the bandgap permits defects with transitions that correspond to absorptions and emissisions within the visible spectrum.

The band structure also provides a representation of the phenomena of surface-induced NV charge state transitions. In other words, the band diagram demonstrates how the modification of the surface chemistry can achieve bespoke concentrations of specific NV charge states near the surface. Therefore, by tuning to mixtures of hydrogen/oxygen terminations we can convert between the NV^+ , NV^0 and NV^- states as shown in Figure 1.5.2 in the near surface region.

The oxygen termination provides the diamond surface a positive electron affinity and no dipole field which leads to a smaller bend bending at the surface in atmosphere. This leads to a majority of NV centres in the NV^- and NV^0 state throughout the near surface region. By comparison, hydrogen terminating the diamond provides the surface with a negative electron affinity as shown in Figure 1.5.2. The negative electron affinity leads to a dipole moment over the CH bond in Figure 1.5.2b and elongates the depletion zone allowing for movements of NVs into the NV^0 and NV^+ states shown in (d). The larger band bending in the hydrogenated state also causes the intersection of the Fermi level with the valence band. This intersection represents the formation of the 2DHG which provides the hydrogen-terminated diamond with its surface conductivity.

The movement of these bands downwards from the hydrogen-terminated state to the oxygenated state will be induced and measured in this work as the tuning parameter for sensing. One can further understand this procedure as tuning the Fermi level to intersect with the NV transition levels at the depth of the NVs in the bulk. Therefore, the NVs probabilistically sit between either two NV states and respond to external fields readily by transitioning between charge states.

The process of moving between the hydrogenated to oxygenated state is also shown for NVs with two depth profiles, those created from 2keV and 4keV implantation energies in Figure 1.5.2 (d). The blue and pink boxes corresponding to the 2keV and 4keV implants and display two very different equilibrium concentrations. Explicitly, the 2keV moves from NV^+ to NV^0 populations whereas the 4keV moves from NV^0 to NV^- populations. These two regimes correspond to two different sensing modalities, single and dual charge state sensors. We will discuss these sensor modalities more in the context of literature in the next section.

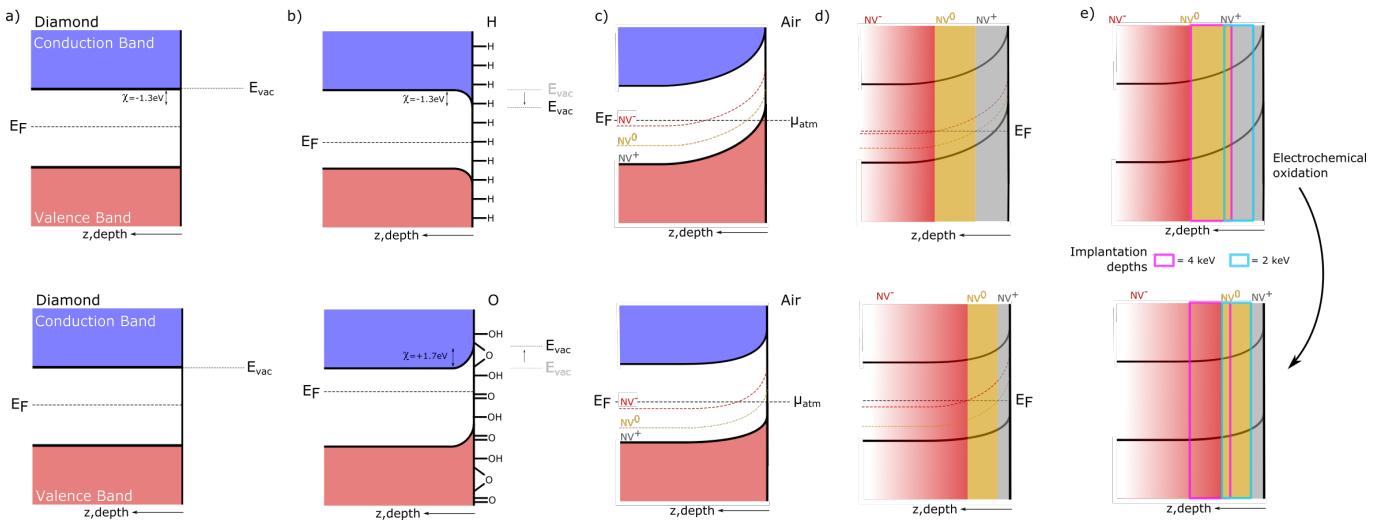


Figure 1.5.2: How the diamond surface termination affects the band bending and therefore the near-surface NV defects. The top row represents the hydrogenated state and the bottom row represents the oxygenated state. (a) The diamond surface is in vacuum and not in equilibrium. (b) The equilibrium state with the termination but not with the atmosphere creates a dipole moment at the surface. (c) When exposed to air the dipole moment created by the hydrogen causes a greater bending up, whereas oxygen doesn't have the same dipole moment and bends significantly less. (d) The effects on near-surface NV centres for a 4keV and 2keV implantation (in reality, the distribution is more complex, the boxes only provide a rough guide).

Finally, the band diagram also elucidates how the sensing mechanism works. For example, with a 2 keV sample ions at the surface of the diamond induce a further bending of the bands resulting in transitions between the fluorescent NV^0 state and the dark NV^+ state. In Figure 1.5.3 this is simplistically shown by the presence or absence of light intensity in response to differing surface charge polarities. The collection of ions at the surface causes a bending of the bands but acts on a much smaller scale compared to electrochemical methods (although the effect is exaggerated in Figure 1.5.3). Yet this band bending from ions at the surface is measurable and reflects the density and polarity of surface charge on the diamond.

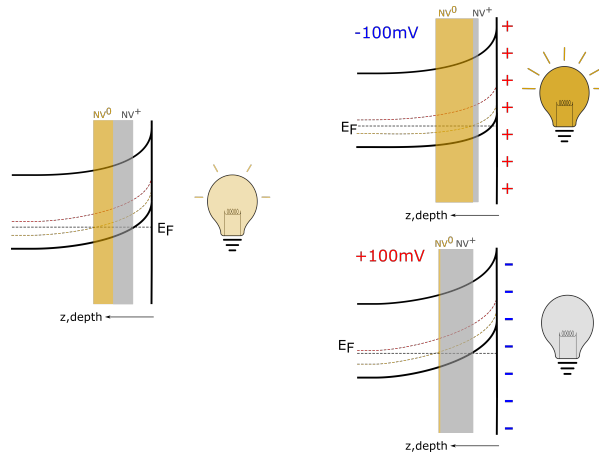


Figure 1.5.3: The sensing mechanism as represented by the band diagrams. The change in the band bending as a result of a surface charge build up leads to a change in the charge state populations and therefore overall fluorescence.

We turn now to critically discuss the existing efforts in the literature for voltage sensing using NVs. By critically analysing these efforts we can further develop our understanding of the sensor and provide a reference for the tuned voltage sensors developed in this work.

1.6 Sensing using near-surface NV centres

We will discuss two key demonstrations of voltage sensing using NVs that are published at the time of writing, a demonstration in nanodiamonds (diamonds of nanoscale dimensions) and single crystal (as discussed in this work).

1.6.1 Nanodiamond electrical sensing

Karaveli et al. have most recently demonstrated the NV centre's sensitivity to its electrical environment by studying NV centres in nanodiamonds (NDs) [11]. They placed hydrogenated NDs (covered in $-H$) and hydroxylated NDs (covered in $-OH$) on an indium titanium oxide (ITO) coverslip, and applied potential fields around the nanodiamonds ($\pm 0.75V$ bias) against a counter electrode in an electrolyte solution. They measured the fluorescence of individual NDs and noted a wide variation in fluorescent responses. However, the majority of the NDs provided responses commensurate with NV charge state transitions. These different fluorescent responses depended largely on the surface termination and so we will consider the hydroxylated and hydrogenated NDs separately.

Hydroxylated NDs: NV^- to NV^0

For the hydroxylated NDs, Karaveli exposes a switching between the NV^- and the NV^0 state. As both the NV^- and NV^0 fluoresce in a similar wavelength range the distinction of the two states was achieved by using a 650nm long-pass filter to collect the longer wavelength fluorescence from the NV^- state (avoiding fluorescence from the NV^0 state). Further spectroscopic measurements cemented this idea showing that as expected there was a clear reddening in the fluorescence when negatively applied fields were provided. In fact they reported a 24% change in fluorescence over a 750mV change in the applied bias.

Sensing electric fields using hydroxylated NDs and a filter ignores the contribution from the NV^0 state. However, in this case the change in charge state population can now be measured in two areas of the electromagnetic spectrum, this means we have a dual measurement system. This dual measurement system would allow for two simultaneous measurements of the NV populations and therefore their electrical modulations. Karaveli notes that at a net-zero bias, there was a spectral contribution of 75% NV^- and 25% NV^0 , a useful point of reference for a later exploration.

Hydrogenated NDs: NV^0 to NV^+

For the hydrogenated NDs, as a positive potential was applied to the diamond via the ITO cover slip there was a reduction in fluorescence. The reduction in this case was attributable to the transition from the NV^0 to the NV^+ state. Interestingly, these modulations were reported to be more uniform and more appropriate for sensing applications in comparison to the hydroxylated case. It is also expected that one will be able to derive a greater contrast from no longer requiring a long pass filter which cuts the fluorescence read out. This ensures that as much light intensity is collected helping to reduce shot noise. With this added intensity, Karaveli was able to report a 110% change in the fluorescence between applied biases of -750mV to 750mV.

However, in both of these cases changes were only ever developed for one polarity at the surface. In other words the nanodiamonds could sense negative or positive ions at the surface, depending on

the surface, but not both. In real sensing applications this will cut sensitivity for example with biological specimen typically operating between -50mV and +80mV.

Furthermore, the results discussed here were also only for a certain proportion of NDs and within this proportion there was a further variance in the exhibited responsivity. These differing responsivities provide significant challenges as to calibration protocols and implementation for uniform sensing. Finally, and most importantly, the voltage ranges that were measurable in this case were far from biologically relevant measurements. For NV implanted NDs to compete with existing sensing technologies significant innovation needs to be undertaken to improve their sensitivity to applied potentials.

The benchmark that Karaveli et al. provides is NV implanted NDs that present no photo-bleaching limitations, a major differentiator from existing VSDs. They reported a maximum response from their hydrogenated NDs of 110% change in fluorescence over a 1.5V potential window, within this work we seek to improve upon this response with a uniform sensing response across a single crystal diamond sample.

1.6.2 Single crystal sensing

Nanodiamonds have large variability in their orientation, surface functionalization (surface termination) and geometric shape. For a diamond voltage sensor that is reliable and repeatable we may look towards a single crystal sensor alternative. There was work done for single crystals here by Grotz et al. [1] in 2012. Grotz et al. explored the relationship between hydrogen and oxygen terminations on nitrogen vacancy charge state populations. Similar to Karaveli, Grotz used a 650nm long pass filter to measure the NV^- contribution and recorded a 20% change between -500 to 500mV using a solution gated measurement. Grotz also did similar work reporting on the transition in single NV but doesn't report on the fluorescence response quantitatively.

The sensor for a single-crystal diamond works by measuring surface charge build-up on the exposed facet of the diamond. To measure these changes the diamond is immersed in a conductive solution for which ions can redistribute themselves in accordance with local electrical environments. For measuring sensitivity, the electrical environment is controlled by a platinum counter-electrode and a gold contact to the diamond which can bias the diamond and attract either negative or positive ions towards the diamond surface. The negative surface ions leads to near-surface NVs moving to more electro-positive states whereas the positive surface ions moves NVs to more electronegative states. This modulation is the sensing mechanism. Changes to the surface charge lead to a screening space charge in the 2DHG and NV centres which translates to a change in the NV charge states.

Karavali and Grotz both explore the two possible transitions out of the three charge states which may facilitate sensing: $\text{NV}^0 \leftrightarrow \text{NV}^+$ and $\text{NV}^- \leftrightarrow \text{NV}^0$. The former we can denote as a single charge state sensor as we can only ever record the fluorescence from a single charge state, the NV^0 . By comparison, the $\text{NV}^- \leftrightarrow \text{NV}^0$, transition may facilitate the recording of both fluorescent charge states simultaneously for example by applying a 650nm dichroic mirror. The two fluorescent signals therefore form a sensor labelled here as a dual charge state sensor. These mechanisms differ slightly so we will formalise them both.

1.6.3 Single state sensor: NV^0 to NV^+

The mechanism for a single charge state sensor considers the transition between the NV^0 and NV^+ state. A positive field on the surface of the diamond brightens the fluorescence where NV^0 states dominate. By contrast, a negative field on the surface darkens the sample as NV^+ states dominate. The change in overall brightness of the diamond provides a measurable signal to indicate the surface charge. The single charge state method therefore requires no use of filters and no spectroscopic

analysis while voltage recording. The single charge state sensor will be the voltage sensor tuned in chapter 2.

1.6.4 Dual state sensor: NV⁻ to NV⁰

The dual charge state sensor uses the transitions between the NV⁰ and NV⁻ states. Instead of having either the presence or absence of fluorescence in the single charge state sensor, the fluorescent profile now changes by shifting its intensity distribution from one side of the visible spectrum (e.g NV⁰ at 500-650nm) to another (e.g NV⁻ at 650-750nm). The NV⁰ to NV⁻ charge state transition works similarly to the NV⁰ to NV⁺ case except now we need to consider two wavelength bands for sensing. As these bands are unique for each charge state, we can therefore read them simultaneously. The simultaneous measurement in these unique bands provides two indications as to any electrical modulations. Not only this but these two signals are anti-correlated; for example a decrease in NV⁻ fluorescence should correspond to an increase in the NV⁰ fluorescence. Due to the overlap in the spectra of NV⁰ and NV⁻ this sensitization is not as straight forward. Attempts to restrict fluorescence measurements to wavelength ranges where only NV⁰ or NV⁻ fluorescence contributes (and not both) leads to lower overall counts. However, due to the anti-correlation between the two signals common noise such as laser noise can be filtered out. Furthermore, we can incorporate other signal processing techniques, such as Bayesian inference to minimize spurious noise such as shot noise. The combined effect of these post-processing methods may therefore facilitate a greater sensitivity overall compared to a single charge state sensor.

To truly understand the value of these sensing modalities and the performance of the voltage sensor we need to define metrics. We will explore three metrics for the investigation covered in this thesis, the fluorescence, contrast and sensitivity.

1.6.5 Sensor metrics

Fluorescence

The fluorescence of a device is characterised in two ways throughout this thesis. Firstly, understanding the total fluorescence intensity profile as a function of the wavelength provides important metrics on the relative populations of fluorescent NV states. For sensing applications, this is important when discussing diamond devices that are dependent on different wavelength bands to sense such as in dual charge-state sensing. Secondly, we can measure the total intensity of the diamond fluorescence. The total intensity is the main sensing mechanism for single charge state sensors and reports correlates to the performance of the sensor directly. Too dim and relative signals will be hard to measure with shot noise limiting the ability of the device to function. Too bright and changes in the fluorescence may be drowned out by the rest of the chip and hard to discern. We can mathematically represent this trade-off by calculating the change in total fluorescence relative to the total fluorescence at some baseline,

$$\tilde{F} = \frac{F_V - F_0}{F_0} = \frac{\Delta F}{F_0}. \quad (1.6.1)$$

Here, F_V corresponds to the fluorescence from an applied electrical signal, and F_0 corresponds to the fluorescence with no voltage applied (i.e zero bias) and \tilde{F} corresponds to the percentage change in fluorescence. There is therefore an optimum total fluorescence in between too dim (small ΔF) and too bright (large F_0) for the use case of sensing electrical signals. It is worth reminding that Karaveli reported a maximum of fluorescence change of $\tilde{F} = 110\%$ while Grotz reported a maximum fluorescence change of $\tilde{F} = 20\%$. However these were in response to differing applied biases. To take these biases into account we need to consider the contrast.

Contrast

The contrast is similar to that seen in a video or a picture, how bright are the light components compared to the dark. Put another way, how well are edges in the picture able to be discerned as shown in Figure 2.5.9d

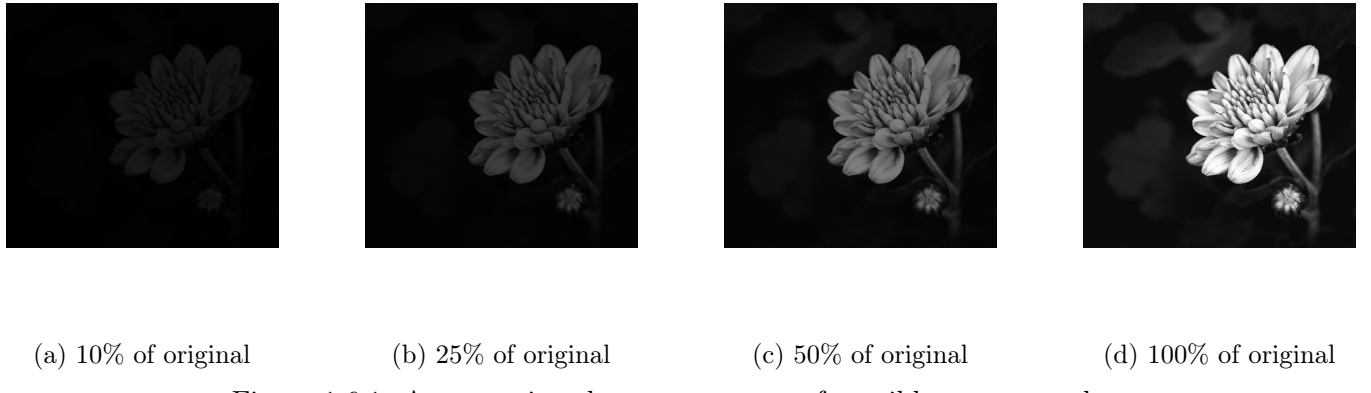


Figure 1.6.1: A comparison between a range of possible contrast values.

In the case of electrical sensing, contrast is measured as the relative fluorescent response, \tilde{F} , to a change in electrical bias across the diamond. Put another way, the contrast measures how large the percentage change in fluorescence is as a result of a change in the electric potential across the diamond. Revisiting Eq. 1.6.1 we now quantify the contrast as the relative change in fluorescence for a given change in the voltage across the diamond as

$$C = \frac{\tilde{F}_V - F_0}{F_0} / V = \frac{\tilde{F}_V}{V}. \quad (1.6.2)$$

Eq. 1.6.2 gives a percentage change in fluorescence per applied bias. Using this definition and the results from Karaveli and Grotz, we can calculate their contrast values as a baseline for the tuning executed in this work,

$$C_K = 0.073\%/\text{mV} \quad \text{and,} \quad C_G = 0.02\%/\text{mV}. \quad (1.6.3)$$

Here, C_K corresponds to the Karaveli contrast and C_G corresponds to the Grotz contrast. However, electrical signalling is not constant in time. The most important application of the diamond voltage sensor is for taking real-time video of electrical activity. For quantifying a sensors temporal resolution we can introduce a new metric: the sensitivity. The sensitivity not only provides a measure of the temporal resolution but is also a useful criterion for comparing to existing voltage sensing technologies.

Sensitivity

Contrast is a measure of how clear a single image is but for the most interesting applications, video imaging, we need to quantify the temporal resolution. The sensitivity is concerned not only with the size of the fluorescent response but the speed at which this can be discerned. For mammalian neurons for example, an action potential persists for approximately 1.21 ms (full width at half maximum) [30]. The sensitivity of the devices characterised here can be quantified by additionally considering the exposure time required to achieve the image over that timescale. The shot-noise

limited sensitivity, η , that case is given by,

$$\eta = \frac{1}{C\sqrt{F_0 f}} = \frac{\sqrt{T}}{C\sqrt{F_0}}, \quad (1.6.4)$$

where C is the contrast, F_0 is the average fluorescence, T is the exposure time and f is the sampling frequency of the imaging device. The sensitivity can feel counter-intuitive as a metric because, contrary to the contrast, we are always seeking to minimise the sensitivity. We want to be able to measure the lowest possible signal. The required sensitivity for measuring intracellular action potentials from mammalian neurons (that is measuring the change of potential inside the neuron) has been calculated by the research group as $0.894 \text{ mV}/\sqrt{\text{Hz}}$ as 1 kHz . This provides the first benchmark required for reaching biologically relevant sensing and will be the first target set out in this thesis.

Chapter 2

Electrochemical oxidation for tuning a diamond voltage sensor

The following chapter presents the techniques used to electrochemically oxidise a diamond voltage sensor to achieve a maximal fluorescence response to an applied voltage. We explore the electrochemical oxidation from the perspective of a diamond voltage sensor operating as a single charge state sensor (NV^+ to NV^0 transition) and tune the surface termination to achieve NV concentrations for biological sensing.

2.1 Preparing the diamond voltage sensor

Before we tune the diamond for sensing applications the diamond needs to be implanted with nitrogen vacancies, patterned with metal contacts and hydrogenated. Starting with electrical grade diamond the $50\mu\text{m} \times 2\text{mm} \times 2\text{mm}$ wafer is implanted with nitrogen at energies of 2keV with a dose of 10^{13} atoms per cm^2 (INNOVION). After annealing at temperatures up to 950° , approximately 1% of the substitutional nitrogen atoms form nitrogen vacancies (leading to an approximate areal density of 10^{11} NV centres per cm^{-2}). Following this anneal, the diamond is then evaporated with titanium and platinum to form metal contacts. The evaporation was done using a positive photoresist to create bespoke patterns for oxidation and sensing. As the samples are small (square of side length between 2mm and 4mm) this relies on a careful spin coating of photoresist followed by a masked exposure to UV and heat to crosslink sections of the photoresist. The delicate nature of the photolithography process was due to the inconsistent areal density of photoresist due to the small area and high viscosity causing significant edge bead on the outer edges of the diamond. Alternate methods were trialled, for example constructing a protective mask (made of Invar) by using a laser cutter and potentially using Electron Beam Lithography (EBL) throughout this thesis.

Once the electrical contacts are on, the next step is the hydrogen termination. The two methods used for the samples in this thesis were microwave plasma and thermal hydrogenation. Microwave plasma hydrogenation requires the sample to be loaded into a microwave plasma enhanced chemical vapour deposition (MPE-CVD) reactor with a molybdenum cage to protect the diamond from the most ionising components of the plasma (which may etch away at the surface). After evacuating the chamber down to a pressure of approximately 13 mbar the chamber is filled with H^2 and N^2 . After heating the molybdenum stage to 750°C a hydrogen plasma is created using 1300W of microwave power and maintained by a 600W of microwave power. The sample is left for 7 minutes before allowing it to cool down. Although the process provides good hydrogen termination, the process is extremely sensitive to any oxygen leaks within the system. Even small leaks can lead to etching and a corrupted surface where metal contacts can no longer adhere to the surface. The peeling of metal contact is speculated to be due to the lack of a strong titanium carbide bond in favour of oxygen related bonds. After these difficulties, work was done to explore alternate methods that were even less destructive and less susceptible to failure.

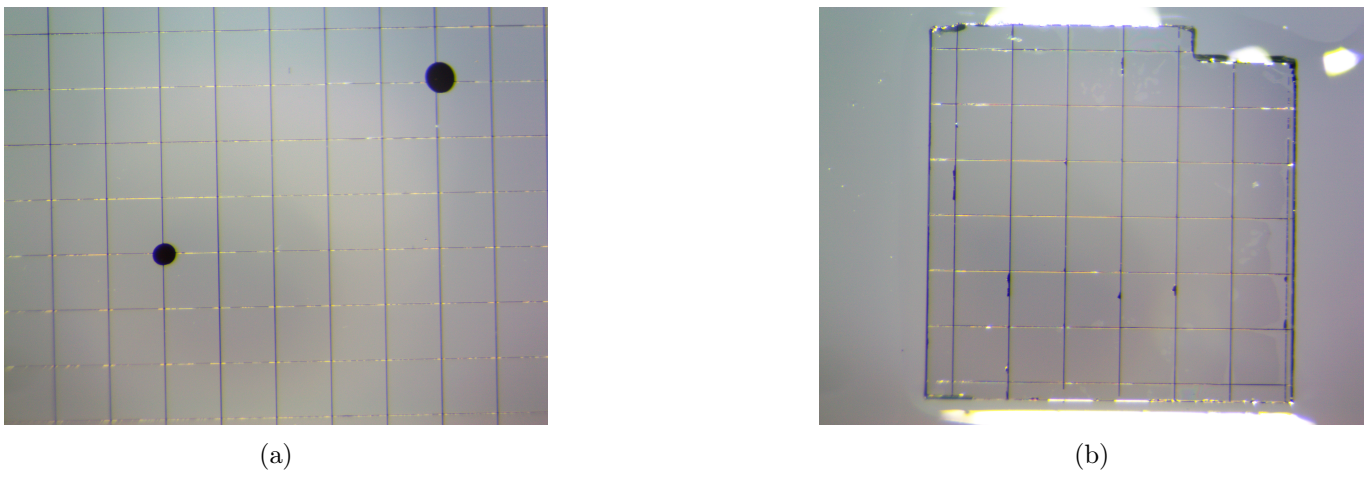


Figure 2.1.1: An image of two samples after their electrical contacts have been evaporated onto the surface.

Thermal hydrogenation was trialled as an alternate method of hydrogen termination so that a dependency on the microwave plasma technique could be removed. The process consists of heating a chamber filled with hydrogen or a hydrogen argon mixture to temperatures of 750-900°C while the diamond is kept out of the hot zone of the furnace until the set temperature is reached. Below 200°C the atmospheric oxygen does not have enough energy to oxidise the surface of the diamond. Above 700°C any oxygen radical species interact with the hydrogen to form water vapour. We therefore keep the diamond out of the hot zone until the set temperature is reached to avoid the oxygen etching that would otherwise occur. The sample is moved into the hot zone using a pulley system (usually a magnetic coupling) and left to be exposed to the hydrogen gas. Recognizing the need to keep the diamond cool and avoiding exposing it to intermediary temperatures is a novel observation developed in the group. The implantation, patterning of metal contacts, and hydrogen termination all provide a conductive diamond device for voltage sensing however, the performance typically starts very poor. To tune the diamond device to an optimal sensitivity, we can employ electrochemical oxidation.

2.2 Electrochemically tuning the diamond

After the hydrogen termination and conductive surface patterning is established, the surface oxidation can begin. The mechanism discussed in [Section 1.4](#) shows that the hydrogen surface moieties can be detached in favour of alternate oxygen-related species using an electrical current. In other words, provided there is sufficient potential difference across the surface of the diamond to reach the activation energy for $=\text{C}-\text{H}$ to dissociate, the surface hydrogen will detach to make bonds with more electronegative species such as OH^- in solution. The recently vacated carbon bond will then create bonds with other oxygen-related species on the surface such as hydroxyl, ether or ketone groups on the surface. The oxidation process was carried out by applying successive oxidative voltage pulses using a *RIGOL 4150* signal generator. The custom LabVIEW code was developed to provide square voltage pulses of varying amplitude and period to oxidise the surface. Each successive voltage pulse was termed as an oxidation step throughout this investigation. As the oxidation voltage contains several variable components, for example, the resistance in the solution, electrolytic double layer (EDL) capacitance and contact resistance the required oxidation voltage had to be determined experimentally. A rough range of voltages was provided from previous experimental work by Dr Daniel McCloskey and literature provided from understanding electrical wear of BDD electrodes [29] leading to a lower bound of approximately 500 mV. The process outlined here can be seen in [Figure 2.2.1](#) where a hydrogenated diamond is oxidised to form a mixture of terminations on the surface.

At a nitrogen ion implantation energy of 2keV the sample starts with high proportion of

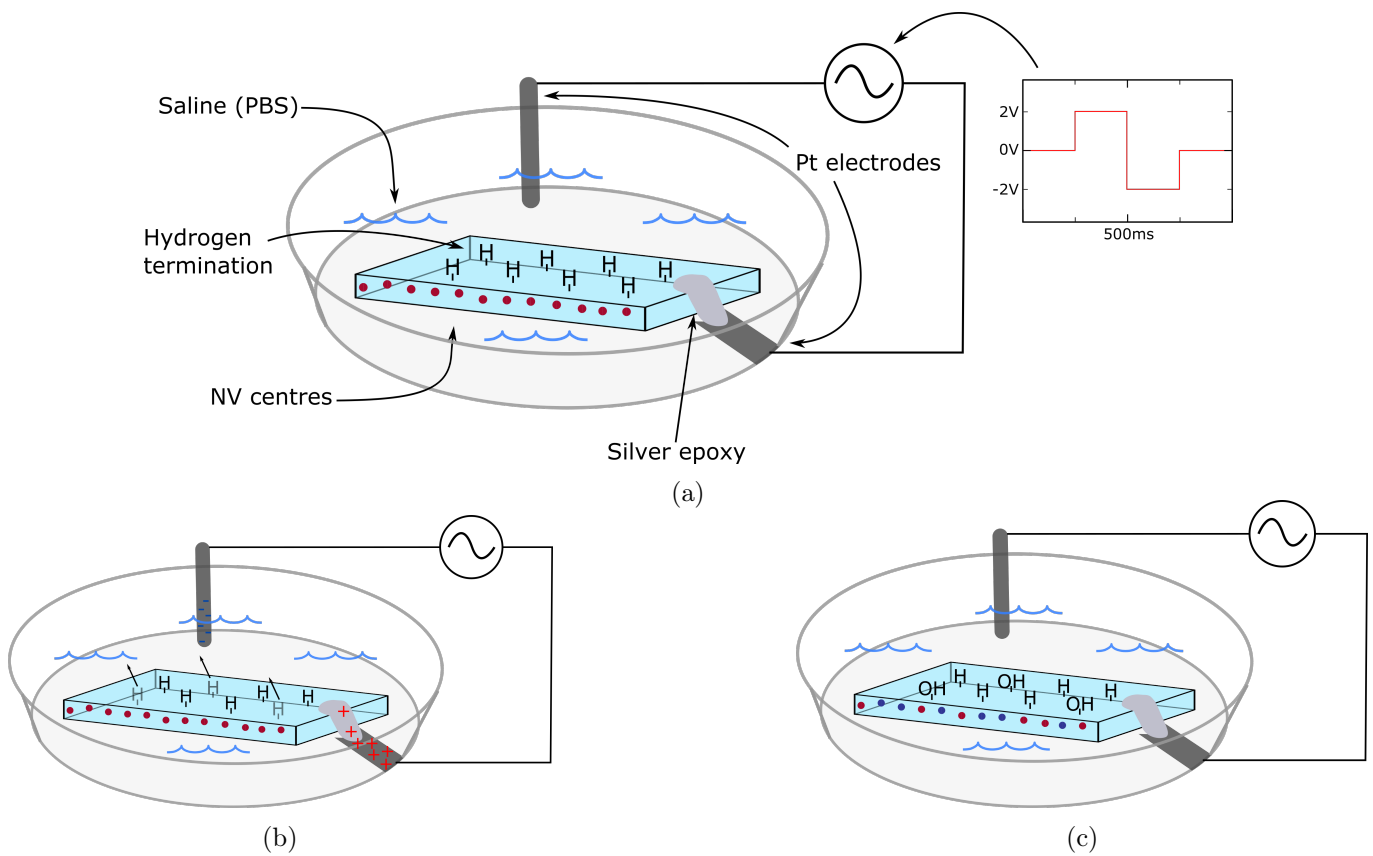


Figure 2.2.1: The electrochemical oxidation procedure. (a) shows the important constituents of the set up for the oxidation procedure. (b) and (c) show the subsequent affects in terms of the flow of charge and the resulting effect on the surface. The burgundy NV centres correspond to NV⁺ states while the navy blue NV centres correspond to NV⁰ states.

NV⁺ states in its hydrogenated state. The predominance of the NV⁺ state therefore causes the diamond chip to become darker in the visible spectrum as shown in Figure 2.2.2.

We expect that through the oxidation process, the original fluorescence from the oxygenated state will return corresponding to the blue curve in Figure 2.2.2. Presently there is no literature on the comparison between electrochemical oxidation techniques compared to other oxidation techniques (such as acid boil or plasma cleaning). The comparison between methods to oxygen terminate the surface will be discussed further in later chapters when NV deconstructions help to demonstrate this comparison.

2.3 Recording Fluorescence

Collecting the diamond's fluorescence efficiently is paramount for maximising the performance of the diamond voltage sensor. We collect the fluorescence with an inverted Nikon Ti-U custom widefield fluorescence microscope set-up, with the diamond illuminated using a 532 nm Verdi laser with a power of 150 mW. There is also an acousto-optic modulator (AOM) which is used to turn the laser off during oxidation of the surface as well as providing a laser-off window to record background light from the laboratory environment. After the AOM, the laser is then reflected off a dichroic mirror and aimed at the back of the diamond. In response to this illumination the NV centres fluoresce and this fluorescence is then collected through the same dichroic and guided into the spectrometer using an optical fibre. A schematic of the optical set up can be seen in Figure 2.2.3.

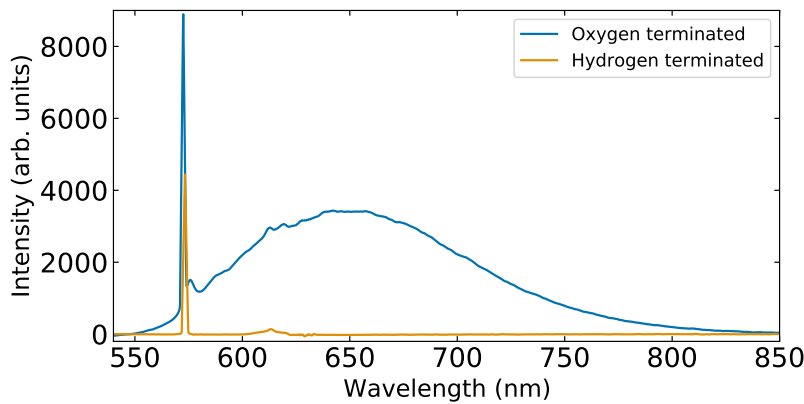


Figure 2.2.2: The spectrum of the 2keV implanted sample before and after hydrogenation. There is an artifact from the glass cover slip that has been removed in the range 625-635nm.

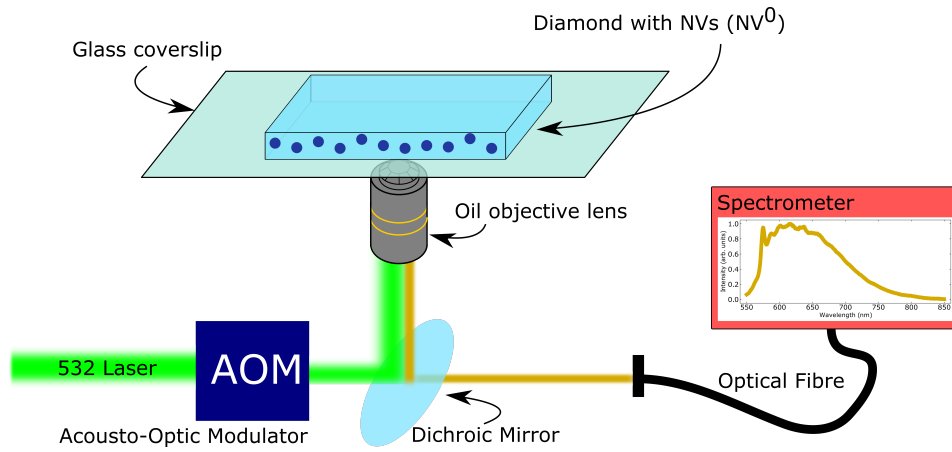


Figure 2.2.3: The optical set up for collecting the fluorescence from the NVs in the diamond.

2.4 Diamond characterisation

After each oxidation step, the effect on the diamond was quantified by recording the fluorescence of the diamond using an *Oceans FLAME* table top spectrometer. The use of a spectrometer provides the ability to verify that the light intensity recorded was in fact from the NV^0 centres as opposed to other sources (e.g the diamond, glass coverslip or oil). The fluorescence was passed to the spectrometer through a 580nm filter to remove the laser illumination and the Raman line of the diamond. We expected any inclusion of the Raman line to reduce the overall contrast (increasing average fluorescence, F_0 , with no gain in relative fluorescence changes ΔF).

Throughout the oxidation we expect the diamond to get brighter. As hydrogen is removed from the surface of the diamond the bands start to bend down as described in [Section 1.5](#). This leads to the conversion, at the near-surface, of dark NV^+ states into bright NV^0 states which raises the total fluorescence of the diamond. However, the overall fluorescence is not the only way to characterise the diamond. We will also probe the fluorescence response to an applied potential difference following each oxidation. This essentially adjusts the bands up and down temporarily to understand how sensitive the NV centres are to changes surface charge build-up. The values from this measurement will then form the contrast of the diamond voltage sensor as described in [Eq. 1.6.2](#).

2.5 The sensor optimisation

To guide our exploration of how the diamond evolved through the oxidation process we can look at the three criteria for sensor performance: fluorescence, contrast and, sensitivity.

2.5.1 Fluorescence

To verify that the electrochemical procedure did indeed oxidise the surface, we can consider the spectrum before and after the oxidation process in Figure 2.5.1. Figure 2.5.1 demonstrates a large increase in the fluorescence as the dark NV⁺ states convert to bright NV⁰ states.

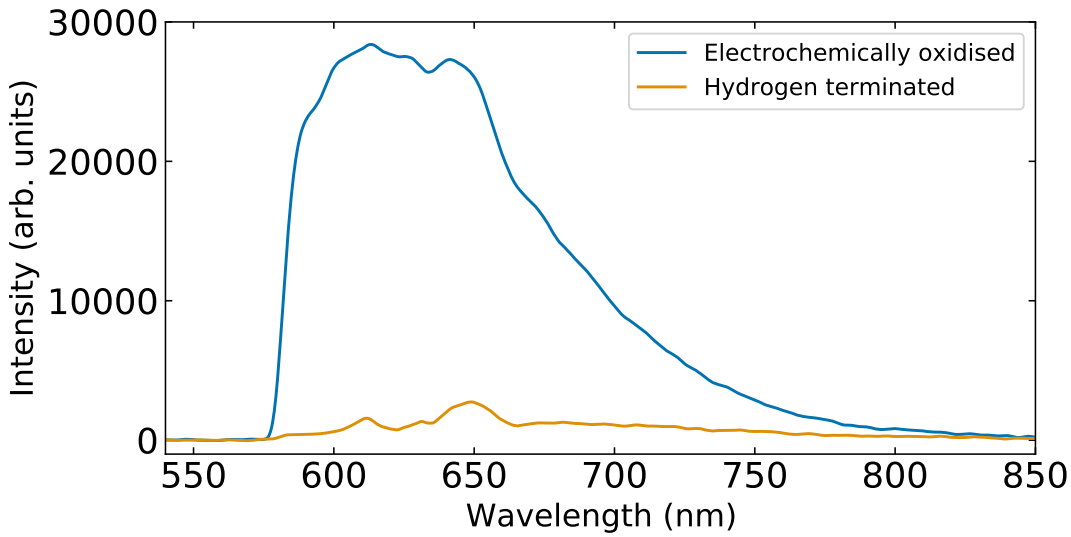


Figure 2.5.1: The spectrum of the same sample recorded through an Oceans tabletop spectrometer before and after electrochemical oxidation. An oil artifact in the 625-635nm range has been removed.

After establishing that the sample gets brighter, we can track this fluorescence increase throughout the whole oxidation process more simply by integrating over the wavelengths to provide an integrated intensity at each oxidation step as,

$$\text{integrated intensity} = \int I(\lambda)d\lambda. \quad (2.5.1)$$

The integrated intensity can then be used to compare the oxidation procedure here with that demonstrated by Hoffman et al.[28] in boron-doped diamond. At the time of writing, electrochemical oxidation has not yet been shown for single-crystal diamond. Figure 2.5.2 demonstrates the first realisation of electrochemical oxidation of single crystal diamond. Despite the differences in procedure, the results manage to correlate well with those shown by Hoffman et al. in Figure 2.5.2b showing that there is a proportionality between the brightness of the sample and the surface oxygen fraction.

In this sense, near-surface NV fluorescence could be used, once suitably calibrated, as an all-optical indicator for how hydrogen-terminated the diamond is. The process is simple to facilitate with a laser and a table-top spectrometer and may provide an alternate measurement for discerning the hydrogen fraction if suitably calibrated.

The shape is largely commensurate with other studies showing a monotonically increasing function as the diamond moves from its non-fluorescent hydrogenated state (NV⁺ dominant) to the fluorescent oxygenated state (NV⁰ dominant). The only deviation from the expected fluorescence is a discontinuity in the curve in Figure 2.5.2a at step 44 and 45. In between oxidation runs, the

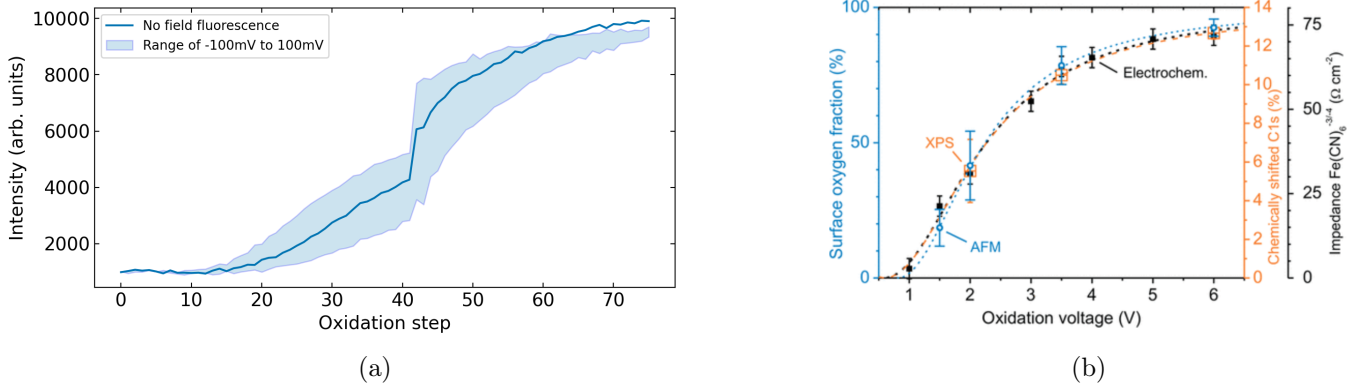


Figure 2.5.2: (a) Integrated intensity (defined in Eq. 2.5.1 of the spectrometer from each stage in the oxidation process corresponding to different total applied voltage and (b) Hoffman et al. measurement of fraction of oxygen on surface measured through AFM, EIS and Raman spectroscopy after exposure to varied oxidation voltage strengths

microscope was refocused by another user and as a result there is an artifact in the shape of a step change in the fluorescence. Interestingly it can be noticed that the positive bias voltages (the bottom of the filled blue area) are not subject to this jump as there was time for the microscope to refocus while negative bias measurements were taken. To clarify this further we can plot the spectra from before and after the refocusing in Figure 2.5.3a and note the marked jump in the fluorescence between the end of the second run and the start of the third run. However, as shown in Figure 2.5.3b, we can scale the change in the fluorescence according to the peak in the phonon sideband of the NV^0 state to see that within the noise of the measurement, the shape is still similar. If still not convinced, we can study the difference between the scaled spectrum and the final spectrum as we only expect the difference to correspond to an increase in the NV^0 fluorescence. In Figure 2.5.3c and notice that it has a significant overlap with a spectrum of just the coverslip and the immersion oil used by the objective lens.

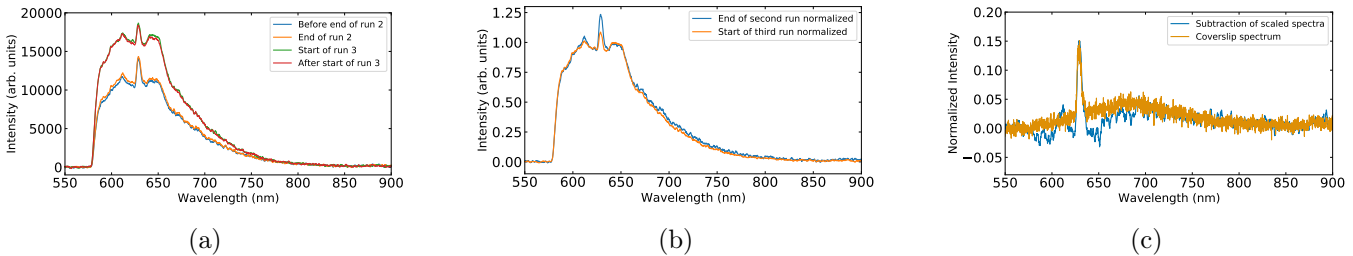


Figure 2.5.3: An analysis at the discontinuous jump in the intensities shown at step 44 and 45 in Figure 2.5.2a. (a) A comparison between the difference in intensity before, during and after the sudden increase in intensity. (b) A comparison of the shapes of the two curves by scaling by the peak of the NV^0 phonon sideband (640nm - 660nm). (c) An overlay of the oil and coverslip spectrum to the scaled difference in the spectra from (b).

The issue corrects itself as the objective drifts into an equilibrium position which aligns with the focus that was used for the rest of the measurement window. The ability to analyse features within the spectrum for troubleshooting unwanted environmental changes is a benefit of using the comprehensive measurement provided by the spectrometer. The inclusion of a Raman line would help to further this troubleshooting as the Raman line is only a function of the diamond and not the NV fluorescence. As such the Raman line could be used for normalising fluorescence measurements

throughout the procedure, for example resolving the refocus issue provided here without a case by case intervention.

Fluorescence provides a good initial understanding of the effectiveness of the oxidation by seeing how the NV charge states in the diamond change throughout the oxidation. In this case, the rise in fluorescence corresponds to an increase in the NV^0 concentration in the diamond. However, to characterise the diamond as a voltage sensor, we need to see how the fluorescence changes as a function of an applied bias: the contrast.

2.5.2 Contrast

To understand the diamond as a sensor, measurements were taken over an array of bias voltages to calculate the contrast of the diamond device after each oxidation step. Here begins the journey not only to understand the electrochemical oxidation as a method to oxygen terminate the surface, but furthermore, to carefully search for an optimal sensing response. We will first discuss the details of calculating the contrast, and its limitations, and then discuss the results of the electrochemical tuning.

Fitting of the contrast

For each oxidation step, the spectrum was integrated to yield a total intensity as described by Eq. 2.5.1. The resulting intensities were plotted against their corresponding bias voltage and the contrast was calculated as the gradient of the linear fit to these points as seen at the beginning, optimal and endpoints in Figure 2.5.4. The applied bias voltage along the x -axis was the bias applied to the diamond meaning that a negative bias on the diamond corresponds to a build-up of positive ions on the surface of the diamond and visa versa for a positive bias.

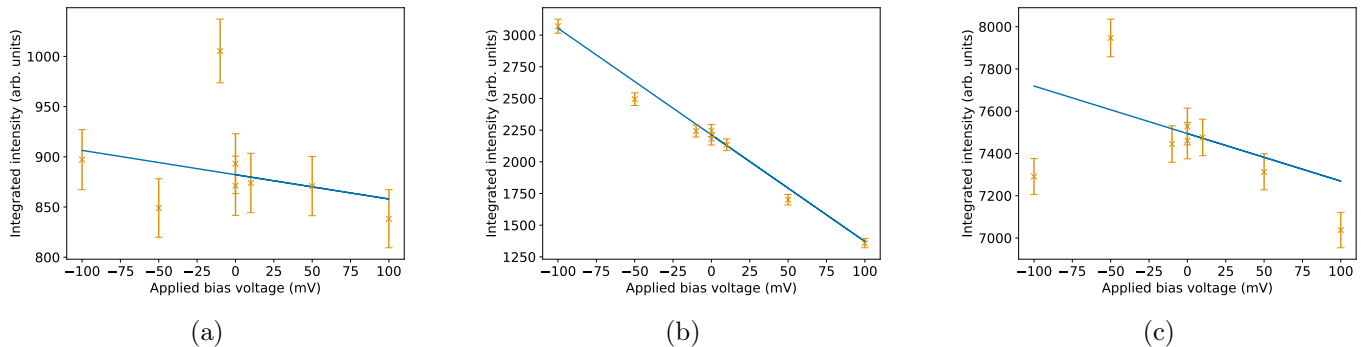


Figure 2.5.4: Fits of the summed intensity compared to the bias voltage applied at the (a) beginning, (b) middle, and (c), end of electrochemical oxidation procedure. The error bars provided are derived from the shot noise error on each point.

The averaging of the sensor response over multiple applied biases forms a more robust estimation of the contrast compared to a single voltage measurement. This is because additional measurements assist in averaging out noise such as laser modulations and shot noise. Furthermore, measuring the fluorescence at multiple bias points helps to comment on the linearity of the response. The gradients of these linear fits are then normalised to the zero-bias fluorescence to provide a percentage change in fluorescence per millivolt. Over the whole oxidation procedure, the linear fits develop an understanding of the sensor performance as a function of surface oxidation steps.

However, an additional note which becomes clear from Figure 2.5.4c is that the response is not linear in poor sensing regimes. By recording voltages only in a small enough window, one can always derive a linear relation. However, the size of this window is dependent on the linearity of the change in fluorescence, and this linearity varies depending on the termination. The breakdown

of this becomes apparent as linearity is not appropriate for sensor responses too far toward the hydrogenated or oxygenated state. The window of voltages chosen throughout this experiment was between -100mV and 100mV as these are commensurate with biological recording. However, it is worth exploring this non-linearity to understand sub-optimal regimes. If we can understand these regimes well, we can successfully predict, during the oxidation, where the optimal regime will lie.

Contrast asymmetry

We will first pursue a qualitative understanding of this asymmetry and follow with a quantitative description by discussing positive and negative contrasts. Positive and negative contrasts will pertain to contrast values calculated only in response to positive and negatives biases respectively. This quantitative description will help to predict the optimal sensor response for future diamond voltage sensors.

Qualitatively we can see the asymmetry in the response through the intensity measurements in Figure 2.5.4c. However, the point can be elucidated further by seeing the spectrum of the diamond with the average fluorescence bias subtracted in Figure 2.5.5. The zero-bias subtracted fluorescence

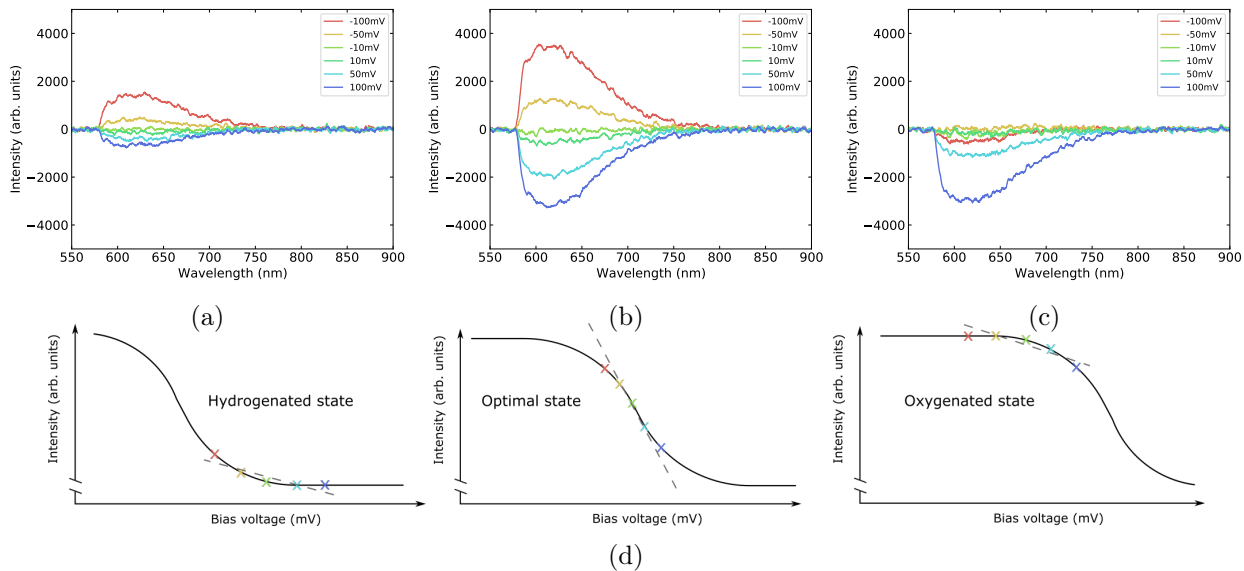


Figure 2.5.5: Sensor response by analysing the fluorescence in response to applying -100mV to 100mV bias voltages with the zero bias response subtracted for the pre-optimal case (step 17) (a), optimal case (step 28) (b), and post-optimal (step 50) (c), sensor responses. Part (d) provides a schematic for the expected fluorescence overlaid with points provided in Figure 2.5.4 to show how the response is not linear for highly hydrogenated or oxygenated states compared to the optimal state.

in the hydrogenated case for Figure 2.5.5a displays the disparity between the response to positive bias (minimal response) compared to a negative bias (large response). The non-linearity is typically less important in these regimes as the overall response is poor for sensing applications as shown by the gradient in the hydrogenated state in Figure 2.5.5d. A similar asymmetry in the opposite direction is shown for the oxygenated state as well however with the opposite response (minimal response to negative biases and large response to positive biases).

The asymmetry in contrast values can be used to the advantage of a sensitizing procedure. Minimal response to positive bias values, Figure 2.5.5a, will suggest a pre-optimum point. Whereas a minimal response to positive biases, Figure 2.5.5c, will suggest a post-optimum point. By quantifying the different responses to positive and negative biases using positive and negative contrasts, future tuning procedures can read out in real time where in relation to the ideal surface chemistry they are

located with greater certainty. Furthermore, as seen in Figure 2.5.6 we can work to a regime where the negative contrast is decreasing to gain a sensor which responds equally between negative biases and positive biases. Finally, by analysing the positive and negative contrasts, it is noted that the optimal termination is different if only sensing in one polarity. In other words, depending on the applications of the diamond voltage sensor, electrochemical tuning can be adapted to achieve greater sensitivity if measurements are only recorded for only positive or negative polarity signalling.

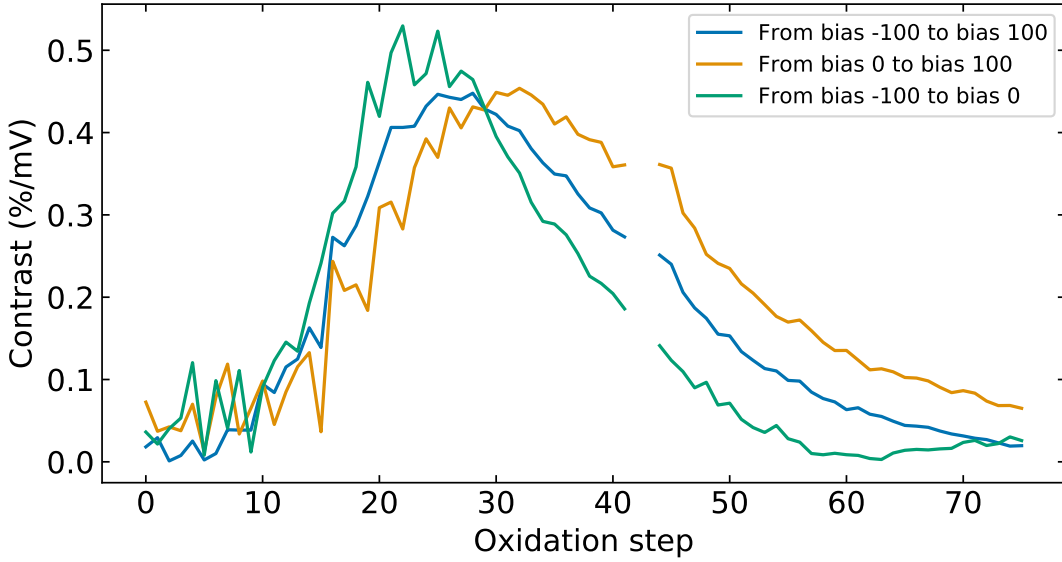


Figure 2.5.6: A comparison between the contrast derived from positive biases, negative bias and all points. The outlier from the refocus issue discussed in Section 2.5.1 has been removed at step 42 and 43.

The diamond voltage sensor's performance

The discussion as to the changes in contrast leads us to considering more deeply the total contrast calculated between -100mV and 100mV shown by Figure 2.5.7. Figure 2.5.7 is a seminal discovery of the work conducted throughout this thesis and therefore we will take time to understand this plot in great detail, and how it will direct further explorations.

The peak in Figure 2.5.7 symbolises the optimal state of the diamond sensor. The contrast peaks at voltage step 29 with a contrast of 0.45 %/mV. To compare to $C_K = 0.073\%/\text{mV}$ and $C_G = 0.02\%/\text{mV}$ the contrast is improved by over 5 times the maximal contrast provided by Karaveli and over 20 times those achieved by Grotz.

An interesting result from Figure 2.5.7 is that the overall shape of the curve is asymmetric. This could be due to two possible contributions. First, there is a trade-off between larger changes in brightness and alongside a brighter average fluorescence. By revisiting Eq. 1.6.2,

$$C \propto \frac{\Delta F}{F_0}, \quad (2.5.2)$$

the response, the numerator ΔF , is drowned out by the overall fluorescence of the chip, the denominator F_0 . The drowning out of the contrast can be seen in Figure 2.5.8 where maximal contrast occurs where ΔF is maximised while F_0 is still below 4000 counts.

The second possible source of the asymmetry comes from the fact that the diamond surface becomes more resistive over the oxidation process. This means that there will be less potential difference provided to the reaction pathway which oxidises surface hydrogen, compared to the potential difference required to traverse the hydrogen termination to the oxidation sites. This is supported

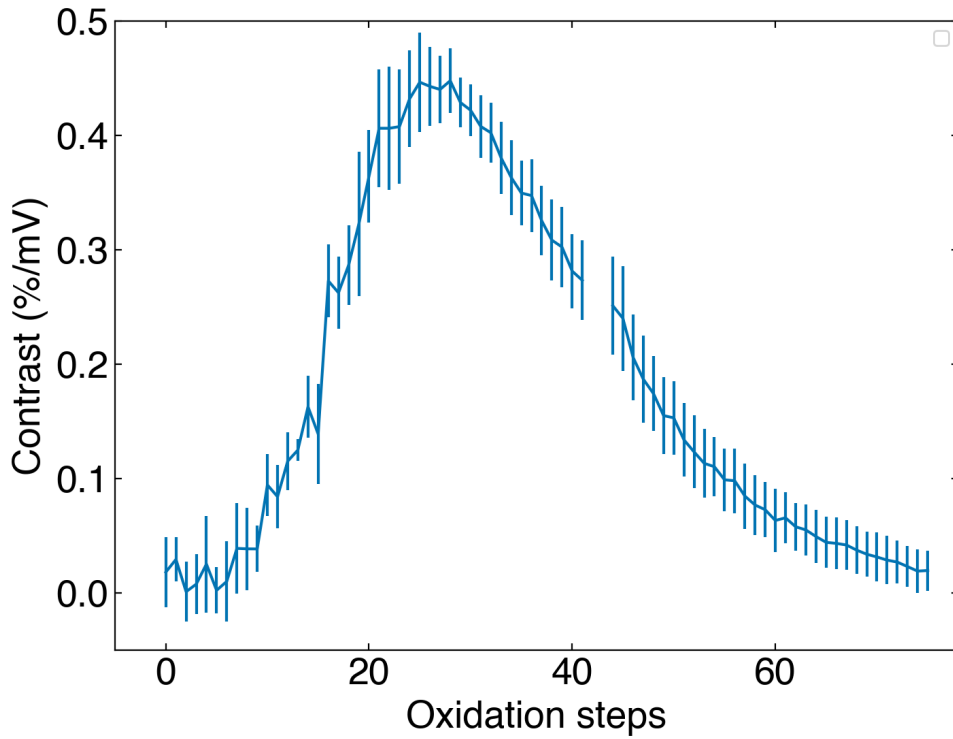


Figure 2.5.7: The absolute contrast. The measure of the fluorescence response to an applied voltage, of the diamond device after progressive oxidation steps of 2V for 250ms (defined as the absolute value of Eq. 1.6.2).

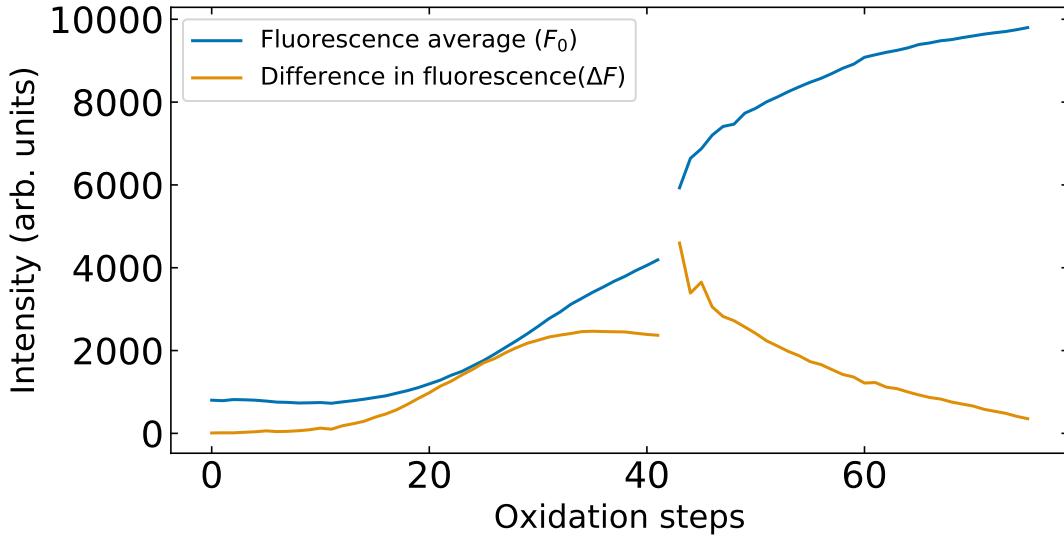


Figure 2.5.8: The numerator, ΔF , and denominator, F_0 , of the contrast calculation. Seeking to minimise the average fluorescence and maximise the difference in fluorescence the optimal contrast can be found at step 29 clearly when the difference in fluorescence peaks. Following this there is a marginal increase in the average fluorescence contributing to a more elongated tail in the contrast plot Figure 2.5.7. The outliers discussed in Section 2.5.1 have been excluded.

by the oxidation by Hoffman et al. in which the reduced efficiency of the oxidation was modelled throughout their procedure [28].

The x -axis, oxidation step, represent an interplay between several different mechanisms at the diamond surface. An understanding of how the hydrogen density is quantifiably varied over the measurement window would be favourable for aligning to theoretical calculations. In this case, with a constant applied voltage a larger portion of the voltage will be dropped across the surface resistance compared to the oxidation reaction. This means that although it is clear that the surface was oxidised, the amount of current contributing to the reaction at each step decreases with the level of hydrogen on the surface. A possible way to circumvent this issue is by considering current sources as opposed to voltage sources which will increase the voltage alongside the increase in surface resistivity.

Finally, as the sensor is operating in an approximated linear regime as discussed by [Section 2.5.2](#), care has to be taken in considering relevant voltages for contrast calculations. For this experiment we chose values between -100mV and 100mV and we can verify the validity of this choice. If the range of voltages selected were too high it would be possible to leave the linear regime and reduce the overall contrast as seen in Figure 2.5.9d. Therefore, if the -100mV to 100mV range was too large, contrasts using the smaller window of 50mV or 10mV will provide a higher maximum contrast. As can be seen from Figure 2.5.9a-c lower bias voltages do similarly if not much worse in the contrast estimates. The lower bias windows also display a large variability from fewer data points and increased sensitivity to shot noise. We are therefore justified in our use of a $\pm 100\text{mV}$ range for calculating the contrast.

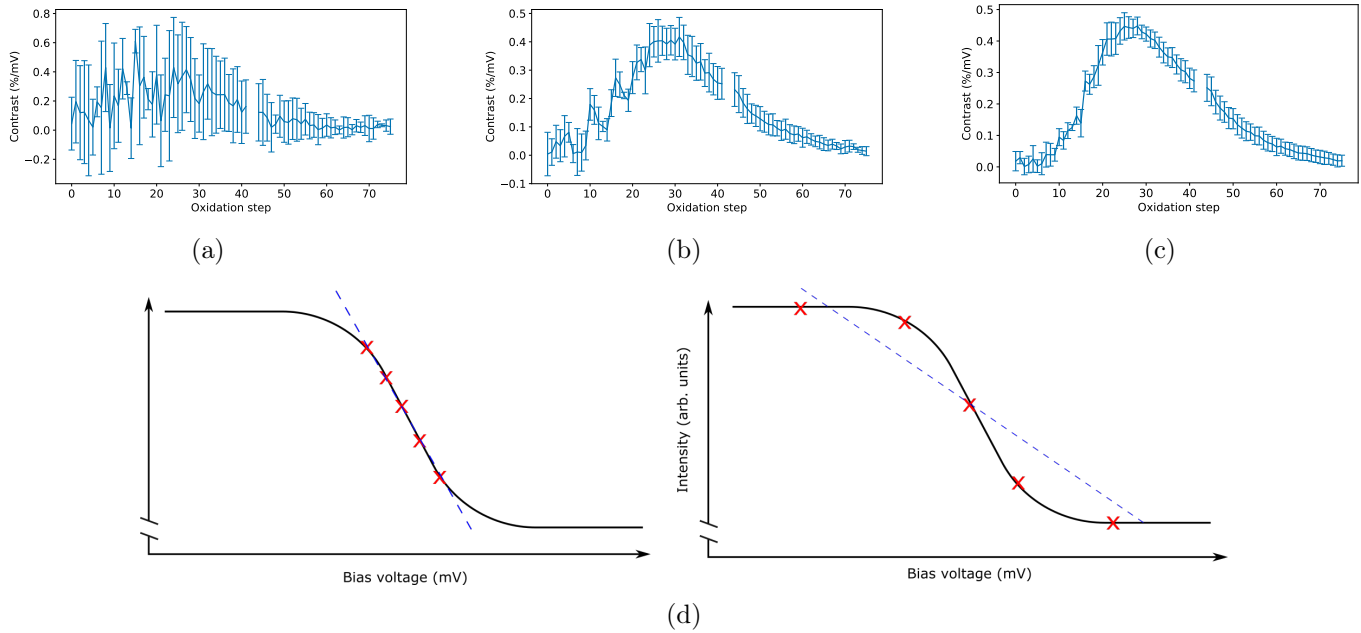


Figure 2.5.9: The contrast calculated between -10mV to 10mV (a) -50mV to 50mV (b) and -100mV to 100mV (c). Note the large variability shown through all 3 plots at the beginning due to the high shot noise in these regimes. The important thing to note here is that the peak contrast value does not decrease when measuring the -100mV to 100mV contrast. Part (d) displays how if the window of bias voltages chosen is too large the contrast (in the form of the gradient) will decrease.

2.5.3 Sensitivity

To finalise our understanding of how the diamond voltage sensor performance progresses, we also consider the sensitivity. The one disadvantage of the spectrometer is its low quantum efficiency requiring a long integration time. However, Figure 2.5.10 still displays a minimum at oxidation step 29 corresponding to an optimal sensitivity, even if the numerical value is a true reflection of the sensor's potential capability. The minimum sensitivity is $346 \text{ mV}/\sqrt{\text{Hz}}$ which is a few orders

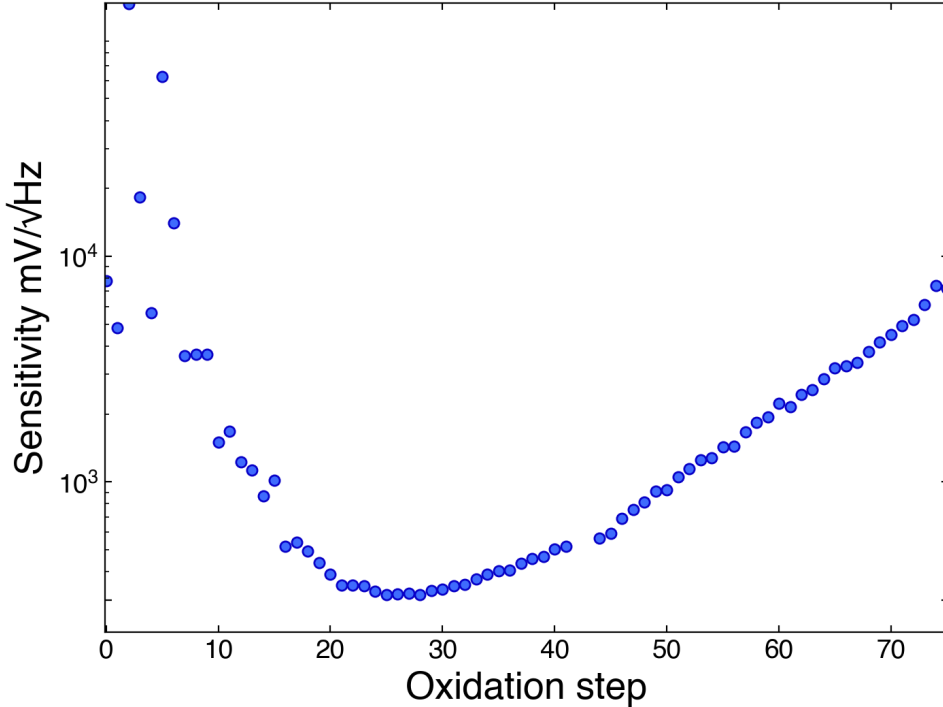


Figure 2.5.10: Sensitivity of the diamond device as a function of oxidation steps. The figure shows a clear minimum, and thus optimal, sensitivity at oxidation step 29.

of magnitude too large compared to many conventional voltage sensitive indicators. However, if provided with a photo-collector such as a photo-diode or a camera we expect the sensitivity of the diamond voltage sensor to be more commensurate with biologically relevant voltages and timescales. Subsequent samples prepared with the same methodology and tuned to their optimal point lead to sensitivities of up to $0.055 \text{ mV}/\sqrt{\text{Hz}}$. With these sensitivities intra-cellular neurons can be comfortably measured requiring sensitivities of $0.894 \text{ mV}/\sqrt{\text{Hz}}$. An additional point of note for the sensitivity shown in Figure 2.5.10 is the flattening out of the curve at it's minimum. The flattening comes from a weaker relationship to the average fluorescence (now a $\sqrt{F_0}$ relation) due to the proportionality of the sensitivity to the sampling frequency. The flattening of the sensitivity around the optimal point makes it easier for an optimal sensing regime to be not be surpassed.

2.6 Conclusion and next steps

This chapter demonstrates an electrochemical method that can be used to sensitize diamond voltage sensors. The optimisation outlined in this chapter demonstrates an improvement of sensitivity by more than a factor of 30 compared to a pure hydrogenated or oxygenated diamond surface. The optimisation provided here, alongside other novel advances by McCloskey et al. [31], could

theoretically reach sensitivities of $0.042 \text{ mV}/\sqrt{\text{Hz}}$. These calculations are provided in a paper, for which the results of this chapter contributes, *A diamond voltagging microscope, Nature Photonics* (accepted 13th of June 2022). These contrast values are commensurate with the sensitivity required for intra-cellular sensing of neurons at $0.894 \text{ mV}/\sqrt{\text{Hz}}$.

The initial proof of concept experiment outlines an effective way of reducing the band bending at the surface of the diamond to optimise an NV⁰ to NV⁺ sensor. This should not be understated as it forms a clear trajectory for optimising diamond devices for novel sensing applications in the future. Furthermore, we investigated the linearity of the diamond voltage sensor throughout the sensitization method with the found the optimal sensitivity also corresponds to the most linear response from the diamond voltage sensor.

Throughout these measurements, the independent variable was a spectrum providing a information as to the intensity of light for different wavelengths. Although this seemed to be the most appropriate way to measure the charge state populations, the low quantum efficiency of the spectrometer incurred a significant time cost as well as providing a poor estimate of the best attainable sensitivity. Yet, we used the features in these spectra at times to troubleshoot issues, such as the refocusing issue, which would not have been possible with a total intensity measurement. To improve our ability to troubleshoot these issues we will include the Raman line of the diamond in future experiments as this feature provides a further reference point throughout the measurement window in it's comparison to the evolution of other features. We therefore require both, a comprehensive measurement of the fluorescent intensity for a given wavelength, and a faster recording of the total fluorescence. The two measurement methods will then provide both an accurate assessment of the sensor capability while safeguarding from unintended environmental changes.

One of the questions that follows from the work in this chapter is how the fluorescence changes for NV centres further into the bulk of the diamond. The main issue here becomes not only how does the fluorescence increase over successive oxidation treatments but also to what extent is this represented in more electronegative NV⁻ states compared to NV⁰ states. For very near-surface NVs represented by the 2keV sample, it can be understood that the transition is predominantly from NV⁺ to NV⁰ and corresponds to either the darkness or brightness of the diamond. However, for NVs deeper in the diamond this is not so straightforward. As both the NV⁻ and NV⁰ centres fluoresce, and overlap in their fluorescence spectra, discerning their respective contributions to a spectrum is not trivial. Previous attempts, for example by Karaveli et al [11], employ an NV⁻ filter restricting recordings to wavelengths of light greater than 650 nm . However, a more sophisticated method may be possible by using the spectra recorded in this method to discern these contributions for sensing applications.

The next chapter of this thesis seeks to address these improvements and points of curiosity. Firstly, we seek to explore alternate oxidation methods, such as using a constant current source, to try and dissipate a more consistent voltage across the surface through the oxidation reaction. Secondly, we will improve upon our methods to characterise the voltage sensor by expanding the spectral measurement window and including camera measurements to better indicate the the voltage sensor's best sensitivity. Thirdly, we would like to explore this oxidation procedure for a deeper implanted sample to see a clearer inter-conversion between the NV⁻ and NV⁰ states. Exploring NVs that are implanted deeper into the diamond will help to develop a picture of how a dual charge state sensor may be optimised. Moreover, the experiment will provide a rich data set which will aid in an attempt to decompose the fluorescence into the contributions from the two charge states, NV⁰ and NV⁻.

Chapter 3

A deeper understanding with deeper NV centres

The following chapter seeks to build on the previous proof of concept by now exploring the optimisation procedure for a dual charge state sensor. The dual charge state sensor is populated with NV centres that are deeper within the diamond. At this depth the NV centres are now subject to transitions between the NV^0 and NV^- state. The optimisation of a dual charge state sensor presents a greater challenge due to the large spectral overlap of the two states and as such we will seek characterisation techniques.

As it has been established that the optimisation technique works, we first explore the limitations of the electrochemical oxidation technique and follow by introducing potential improvements. We turn to questions such as, can using a camera as opposed to a spectrometer give a better indication of the contrast and sensitivity? How does the diamond respond to constant current pulses compared to constant voltage pulses in eliciting oxidation of the surface? and finally, how uniform is the oxidation along the surface? We will follow these questions with the tuning of a dual charge state sensor implanted with nitrogen at energies of 4keV and expected to sense electric fields through changes in fluorescence between the NV^0 and NV^- state.

3.1 Methodology variations

The methodology differs from [Chapter 2](#) in three significant ways, by measuring the fluorescence using a camera as well as spectrometer, changing the delivery of current for facilitating the oxidation reaction, and finally, we consider the uniformity of the oxidation over the diamond surface.

A quick point before jumping into these key methodological explorations is that instead of the titanium carbide and platinum contacts that were used for previous samples palladium was used as an electrical contact on the diamond. A recent publication showed that palladium could be placed on hydrogen-terminated diamond to form electrical contacts [32]. Palladium was hypothesized to be advantageous here as it can be deposited after the hydrogen termination and also boasted a low contact resistance allowing charge to flow more freely between the diamond and the contact in sensitization procedures.

3.1.1 Camera measurements

To provide sensitivity estimates for the sensor which would be more commensurate with the performance of the diamond as a biological voltage sensor, we can use a camera that has a higher quantum efficiency compared to the spectrometer. However, as the camera does not differentiate between wavelength intensities of the received fluorescence, the camera provides information quickly but doesn't distinguish between NV^0 and NV^- fluorescence. To rectify this and only record the NV^- contributions to a potential dual charge state sensor we recorded the fluorescence through a

$709\text{nm} \pm 83.5\text{nm}$ band pass filter. As the contribution to the spectrum of the diamond at wavelengths on or above 625nm is largely due to the NV^- state this serves to measure the contrast of the NV^- state over the oxidation cycle. The camera, with it's better sensitivity, will also be able to discern smaller changes in the brightness of the NV^- state throughout the oxidation process. The additional sensitivity is especially helpful in reporting whether smaller oxidation effects are present with smaller oxidation pulses. Increasing the detection threshold for whether oxidation is indeed occurring becomes crucial for deciding the strength of the oxidation voltages/currents to be applying throughout the measurement.

3.1.2 Current pulses

The electrical impulse provided to oxidise the diamond can be in the form of a constant applied voltage or current. Both of these methods elicit different charge dynamics for the diamond system as to where and how energy is dissipated throughout the circuit. The main issue of the previous oxidation method was that the fraction of the applied voltage which drops over oxidation reactions, decreases as the surface becomes more resistive. Alternatively, maintaining a consistent current through the circuit will see the voltage scale with the increase surface resistivity. Furthermore, current may be useful in quantifying the total injected charge as a unit of measure to provide a consistent dependent variable throughout the oxidation procedure. Injected charge may not always cause an oxidation event if the activation energy is not reached but it still provides a qualitative understanding of the surface oxidation reactions. The injected charge that does not go towards an oxidation event is allocated to charging the surface capacitance made up of the electrolytic double layer (EDL) and quantum capacitance in series. The injected charge that does go towards an oxidation event is referred to as the Faradaic charge. To ensure that current pulses will oxidise the surface and to validate our present understanding of the electrical dynamics of the system we can study an equivalent electrical circuit.

An equivalent circuit

The diamond with its conductive surface contains several components so it is favourable, for our understanding, to represent it through an equivalent electric circuit. This equivalent circuit, uses resistors, capacitors and diodes to represent the different components in the diamond system and aids in modelling the charge dynamics in the system.

From the negative terminal to the positive terminal of the signal generator there is first the journey from the copper in the PCB board through into the silver epoxy and onto the diamond surface the pathways here are absorbed into the variable resistance R_1 . The current travels through the conductive surface layer which becomes more resistive over the life cycle of the oxidation treatment leading to R_1 's variability. The current is then split between two paths. The first path leads to charging the surface capacitance in the device given by the electrolytic double layer (EDL) and the quantum capacitance. The EDL capacitance created from the hydrogenated terminated diamond is created between the 2DHG and the ions on the surface of the diamond and has been recorded at $2 \mu\text{F}/\text{cm}^2$ [33]. While the quantum capacitance is a function of the energy-dependent filling of electronic states in the NV centres and 2DHG [34]. The secondary path is through oxidising hydrogen ligands on the surface of the diamond and therefore requires a certain voltage to become available (represented by the diode). The secondary path is also expected to change throughout the oxidation process as difference surface geometries will require different energy requirements for dissociating specific hydrogen ligands on the surface. At the beginning of the oxidation procedure, the hydrogen groups with low activation energies are removed leaving hydrogen ligands with higher energy requirements for detachment from the surface. Finally, there is an additional capacitance at

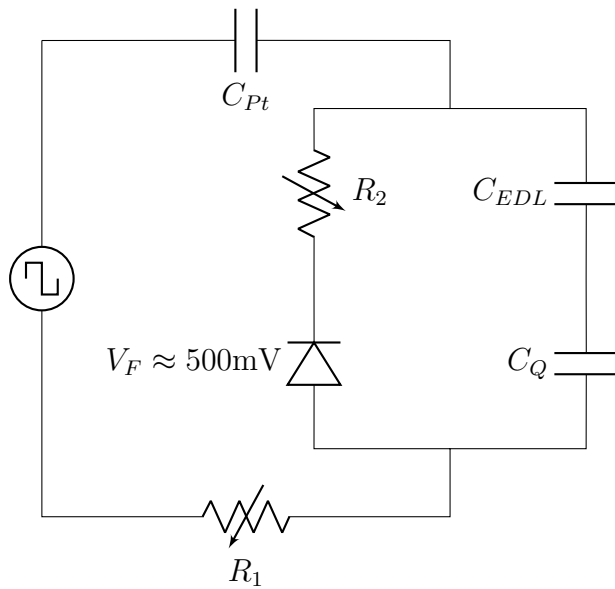


Figure 3.1.1: An equivalent circuit for the electrochemical oxidation system. R_1 corresponds to an amalgamated resistance from the signal generator to oxidation sites on the diamond. C_Q , C_{EDL} and C_{Pt} correspond to the quantum, EDL, platinum and capacitances. R_2 corresponds to the voltage dissipated in the oxidation reaction and the diode represents the required activation energy for oxidation of the surface.

the platinum counter electrode provided by C_{Pt} which can be calculated at approximately $3.3 \mu\text{F}$ [35].

From the Figure 3.1.1 we can see that as long as the voltages from the current pulse exceed the activation voltage, current pulses will still induce an oxidation reaction at the surface. In practice, the threshold voltage for oxidation reactions at the surface is not well known in a PBS solution. As such, we will continue to pursue a similar method of ramping up the current slowly to not destroy the diamond and allow an exploration of what current values elicit reactions at the surface. For the current pulse oxidation procedure, a *Keithley 2450 source meter* will be used to supply a constant current pulse to the diamond. The aim of using this current source is to now provide a voltage across the diamond which scales with the increase in surface resistance given in Figure 3.1.1 as R_1 .

For our final exploration before exploring oxidation for the deeper NV implanted sample, we turn to addressing the uniformity of the oxidation procedure. The discussion above assumes a fixed field of view for the oxidation when in actual fact the oxidation occurs over the whole diamond surface. In ideal cases, the whole sensor may be able to be used for potentiometry measurements as more sensing area improves the minimum total sensitivity. Understanding how the above electrical oxidation is distributed over the entire sample will be our next exploration. The effective range of electrochemical procedure needs to be established so that patterning of electrical contacts over the surface of the diamond can be created to balance maximum sensing area and surface oxidation effectiveness.

3.1.3 Oxidation uniformity

Understanding how this oxidation procedure distributes itself over the whole surface area is important in creating voltage sensors with a uniformly optimised sensing area. Previous work by Hoffman et al. [28] with Boron-Doped Diamond (BDD) showed that islands of hydrogen-terminated sections (of the order of 100 nm^2) will form on the diamond surface, with the number of islands reducing with stronger oxidation voltages. However, the work in this thesis was conducted with a single crystal diamond as opposed to BDD so it would be fruitful to compare these results to see if

similar islands are seen throughout the surface. To address this concern, the contact placed on the diamond surface was placed along one side of the diamond and the fluorescence was then measured at 5 different locations across the diamond. Difference in the fluorescence across these different measurement windows served to track how the oxidation progressed at distances further from the contact.

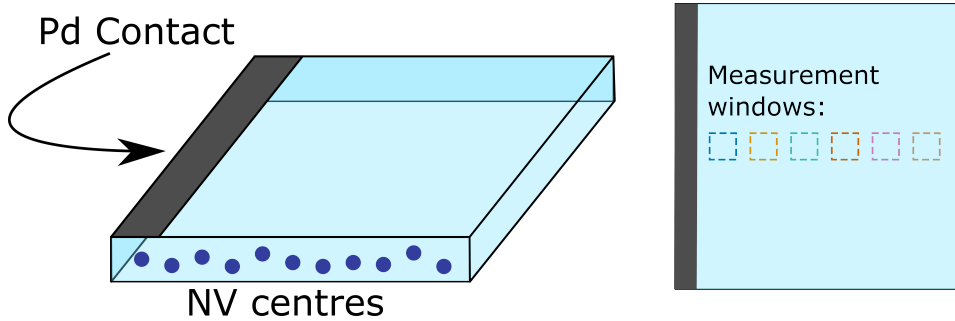


Figure 3.1.2: The schematic of the palladium (Pd) contact on the diamond from the side (a) and from a bird's eye view with the measurement windows.

In Figure 3.1.3 the oxidation can be observed throughout the entire sample by the overall increase in fluorescence. However, the level of oxidation, provided by the integrated intensity is much smaller for distances outside the first window of view corresponding to distance of $300\ \mu\text{m}$ or higher. As a result of this, future dual charge state sensors were patterned with $300\ \mu\text{m}$ grids to ensure that oxidation would be distributed evenly throughout the diamond. It is also worth noting that the larger increase in fluorescence intensity at $3200\ \mu\text{m}$ is due to a higher conductivity at the edges of the diamond. There is a higher conductivity here due to the lack of nitrogen doping causing an increase in the band bending and thus a larger 2DHG. The increase in conductivity of the surface has also been verified in separate experiments using pin-to-pin conductivity measurements of the side of the diamond compared to the surface.

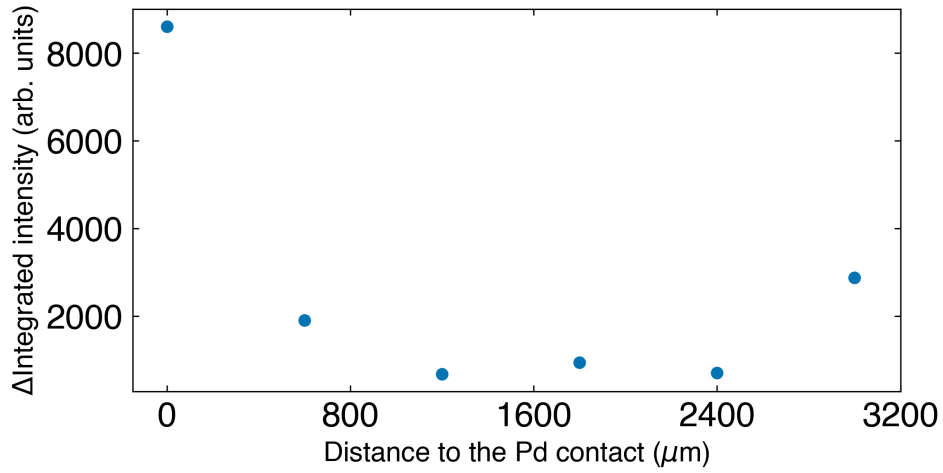


Figure 3.1.3: The change in integrated intensity between the pre and post oxidation states of the diamond sample. The x -axis corresponds to the windows outlined in Figure 3.1.3 which are positioned at different distances from the palladium contact ranging from $0\mu\text{m}$ to $3000\mu\text{m}$. The disparity at the end of the oxidation shows that the oxidation is a short range process occurring at distances less than the field of view (i.e less than $300\mu\text{m}$).

With this more complete understanding of the electrochemical process, we now take these improvements into the exploration of a dual charge state sensor. A dual charge state sensor requires

NVs to sit in a balance between NV^- and NV^0 states and therefore requires the distribution of NVs to be deeper in the diamond. We will first discuss how we characterise this deeper implantation profile and follow with an analysis of how the deeper implantation responds to electrochemical oxidation.

3.2 The deeper implantation profile

Now we look towards a deeper ensemble of NV centres to realise a dual charge state sensor. For a dual charge state sensor, we require the NV centres to readily transition between the NV^0 and the NV^- state. Although tuning leads to some changes in the NV charge state populations, we can effectuate large changes in the NV equilibrium charge states by positioning the NV centres deeper in the diamond. NVs deeper in the diamond are situated within a more electronegative environment compared to NVs closer to the surface (shown in the band bending picture in Figure 1.5.2) and therefore are more likely to exist in the more electronegative, NV^0 and NV^- , states. A deeper charge state population means that the 4keV sample starts with a strong NV^0 population immediately following hydrogenation. A spectrum for each of the sample was taken before and after hydrogen termination and then throughout the oxidation process. Figure 3.2.1 serves as the start and endpoint for the oxidation procedure for the diamond pre- and post-hydrogen termination.

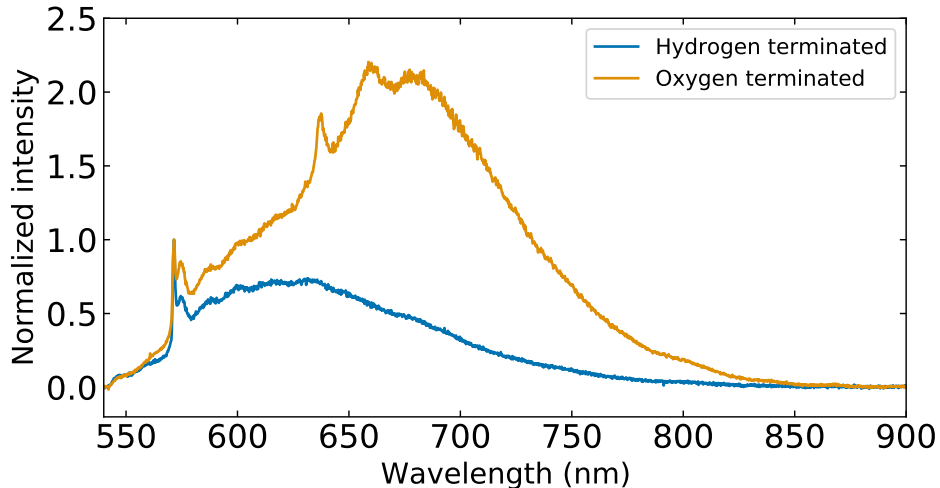


Figure 3.2.1: The diamond fluorescence before and after hydrogen termination for a diamond sample implanted with 10^{13} nitrogen ions per cm^2 of energy 4keV. Both spectra are normalised to the Raman line of the diamond. The hydrogenated case has a lower fluorescence and a shift of the fluorescence predominantly towards lower wavelengths signifying an increase in the NV^0 and NV^+ populations compared to NV^- states.

In Figure 3.2.1, the fluorescence will increase in its longer wavelength contribution, as the surface is oxidised. The purpose of this chapter is to watch this transition in great detail over the oxidation process, testing throughout for ideal sensing responses. For a dual charge state sensor, the ideal sensing mechanism is slightly more complicated, as the contrast and the sensitivities now come from two sources. In any case, it will be closely associated with the contributions to the spectrum at each point from NV^0 and NV^- densities in the diamond.

The discerning of these contributions has been done in several ways in the literature which we can use as a comparison for our analysis. The deconstruction of the charge state fluorescence has been done by differing surface terminations in nanodiamonds [11], by using different laser illumination (as NV^- and NV^0 have different absorption profiles)[36], or by using magnetic field modulations [37]. These examples of discerning the NV charge states contributions can be seen in Figure 3.2.2

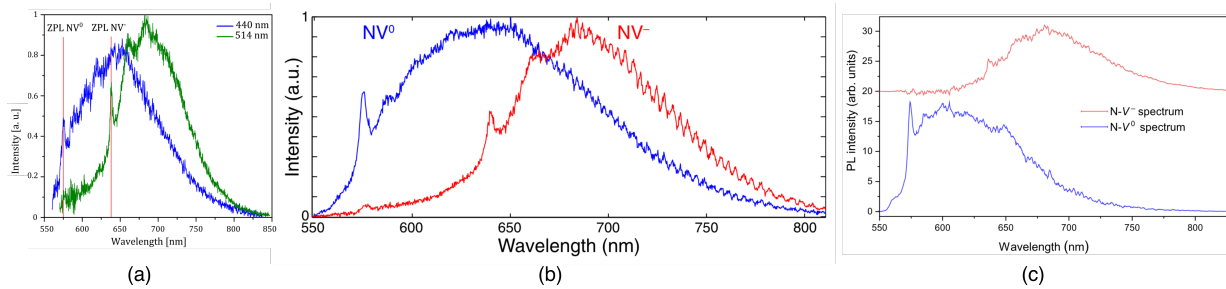


Figure 3.2.2: Experimental derivations of the spectrum of the NV^0 and NV^- state using (a) surface functionalizations and applied voltages to nanodiamonds [11], (b) different wavelength illumination light [36] and finally strong magnetic fields (c) to split up NV charge state population densities [37].

In the following sections we will also develop a software approach to discern these contributions for two reasons pertinent for a voltage sensor. First, the optimal sensing balance can be characterised not only by a total fluorescence profile but also by an $\text{NV}^0 / \text{NV}^-$ ratio. This means we may be able to scan and monitor the charge state populations as a method to tune to an optimal dual charge state sensor. Secondly, a fast spectrometer may be able to use the developed classifications for recognising the NV populations while sensing. There is a large spectral overlap between the NV^0 and NV^- states which limits the ability to sense each of them individually without spectroscopic measurements. However, if a spectral measurement was able to be recorded sufficiently fast, it is possible that processing the spectra with the use of a classifier would promote better total sensitivities.

3.3 The sensor optimisation

We begin our analysis of the dual charge state sensor in the same way as for the original 2keV implantation in [Chapter 2](#) by progressing through our established metrics, fluorescence and contrast. We will then follow this evaluation with a rationale of why an optimal sensing regime was not discovered and follow this with tools to predict optimal sensing regimes in the future.

3.3.1 Fluorescence

To verify that the surface is indeed oxidising we can once again look at the overall increase in fluorescence over the lifetime of the oxidation in Figure 3.3.1.

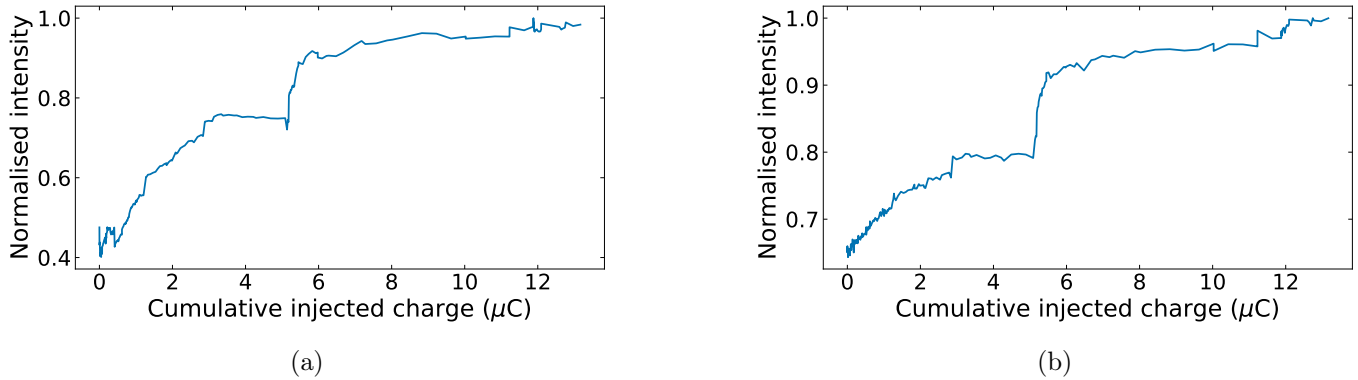


Figure 3.3.1: An initial integrated intensity of the spectrometer throughout the oxidation process (a) and the integrated intensity after scaling to the Raman line in the spectra (b).

The fluorescence increase again supports that oxidation occurred and that a current source was sufficient to facilitate the oxidation. The fluorescence increase should be less than the shallower implant as we already started with a substantial NV^0 population and therefore have less overall

fluorescence to gain. This is made clear in comparing back to Figure 2.5.2a which came from no fluorescence to a total of 10000 counts compared to Figure 3.3.1 which saw an approximate increase of 43% in its integrated intensity.

By comparing Figure 3.3.1a to the Raman line normalised total intensity in Figure 3.3.1b there is an improvement in the shape becoming a monotonically increasing function after scaling. This is most clear in the first $3 \mu\text{C}$. This scaling became instrumental for the data collected as it was taken over a time frame of longer than a month (due to the time required for measurements).

There is once again a noticeable jump in the total fluorescence at approximately $5 \mu\text{C}$ despite scaling by the Raman line measured by the spectrometer. From an initial analysis similar to that shown in Figure 2.5.3a, the jump in total fluorescence can be attributed to a marked increase in the NV^- fluorescence. However, we will seek to formalise this in Section 3.4.3 with a more telling analysis of the spectra.

The camera measurements were not used in understanding the integrated intensity as there was no way to control for the variation in laser noise over long time scales (spectrometer measurements were not exactly simultaneous with camera measurements). Fortunately, as contrast measurements are normalised to the average fluorescence for the camera and the spectrometer, we can still compare the contrast between the camera and the spectrometer.

3.3.2 Contrast

Despite successfully oxidising the surface the contrast steadily got worse and stayed worse throughout the oxidation procedure as shown by both the spectrometer and the camera in Figure 3.3.2.

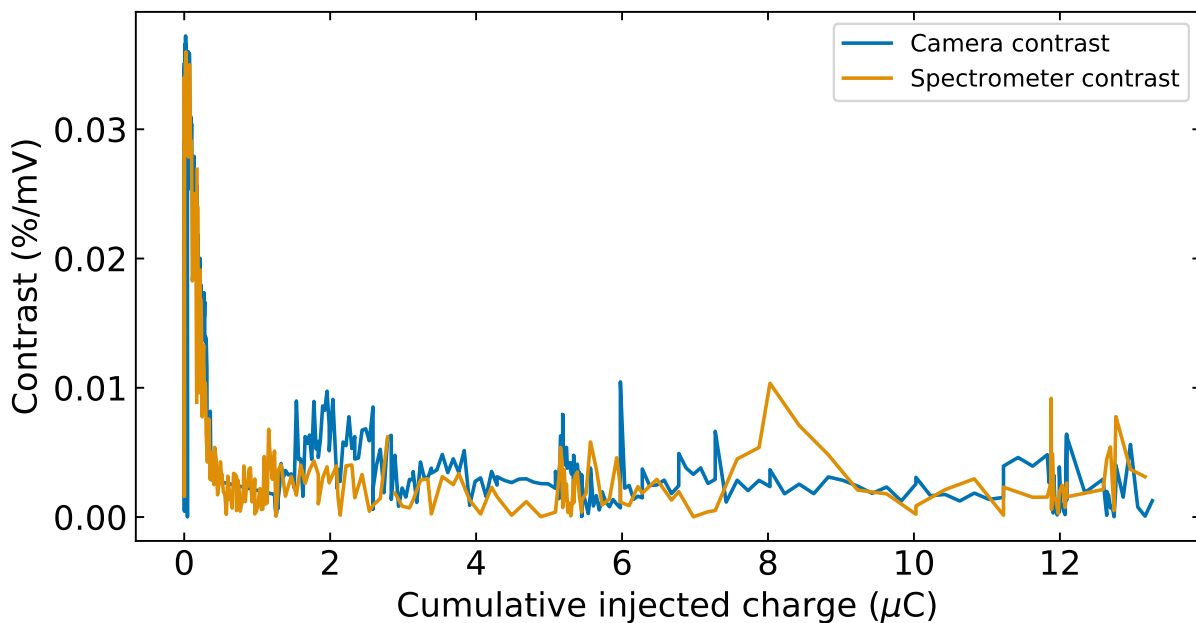


Figure 3.3.2: The contrast as measured by the spectrometer and the camera over the oxidation process, started with a large contrast and then progressively decreased through the oxidation procedure.

As the spectrometer contrast is derived from an integrated intensity over all possible wavelengths, the spectrometer contrast reflects the performance of this sample as single charge state sensor (using NV^0 to NV^+ transitions). For deeper nitrogen implantations the NVs are further into the bulk and therefore require a large band bending effect to transition to NV^+ states. This is

demonstrated in Figure 3.3.2 where the contrast is best at the start of the measurement (with the bands bent up to a maximal state) and then progressively gets worse.

By comparison, the camera has a 625-793nm filter and should be predominantly measuring the NV⁻ fluorescence throughout the measurement as can be shown in Figure 3.3.3. However, the contrast similarly decreases throughout the oxidation process. Initially still measuring a portion of NV⁰ transitions due to spectral overlap, the contrast in the camera still reflects the performance of the sensor as a poor single charge state sensor. Furthermore, despite the progressive oxidation favourable contrasts derived from NV⁰-NV⁻ transitions did not arise.

It was hypothesised that with enough oxidation the decrease in the hydrogen on the surface would lead to applied potentials causing the interchange from the NV⁰ state to the NV⁻ state. For example, in the presence of a strong negative bias to the diamond, we will record the conversion of NV⁰ states to NV⁻ states and an increase in intensities of longer wavelengths within the spectrum. This regime was unfortunately not reached. There seems to be a slight increase in the contrast towards the most oxygenated termination able to be reached using electrochemical oxidation, but this is unfortunately not above the variability seen throughout the experiment.

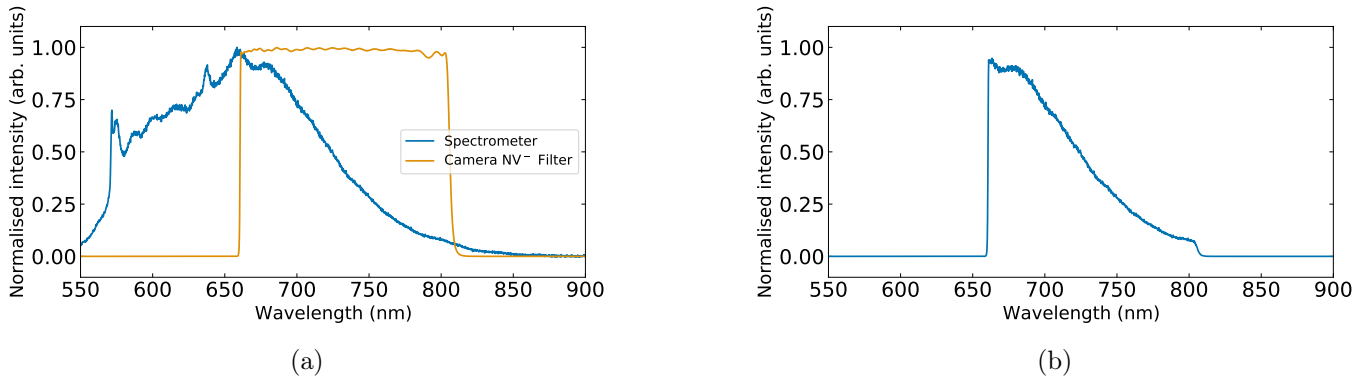


Figure 3.3.3: An example spectrum and the overlay of the filter used for the camera fluorescence (a) and the resultant intensity that hits the camera (according to the spectrometer) in (b).

However, the result shown here is specific to this sample which exhibits a different distribution of NV centres compared to other samples implanted with nitrogen at energies of 4 keV which exhibit a larger population of the NV⁻ state. As can be noticed in the initial oxygenated state the mixture in Figure 3.2.1 of NV⁻ and NV⁰ is further towards the NV⁰ state which may imply that the sample is actually not suitable for dual charge state sensing. To increase the NV⁻ population, we can implant NV centres deeper into the diamond and therefore more likely to exist in the NV⁻ state as can be seen in Figure 1.5.2(d). Due to the lack of contrast for this sample, we will not seek to analyse the sensitivity as it provides, at best, a comparison between the camera and spectrometer.

Instead, we will instead explore the data in two ways. Firstly, the following question quite clearly becomes, if we need the NVs to be deeper for a more favourable mixture of NV⁻ charge states, what depth is optimal for dual charge state sensing. Furthermore, how might we characterise these NV depths? To address these questions we will first develop a method to characterise the NV populations using their fluorescence and then use these results to make projections as to more apt NV concentrations. For estimating the NV population we first need a sophisticated way of isolating the different charge state fluorescence.

3.4 Distinguishing NV fluorescence using Non-Negative Matrix Factorization

For the realisation of a dual charge state sensor, we need to have a quantitative understanding of the presence of the two charge states, NV^- and NV^0 , in the sample. We can estimate these populations by analysing how their unique fluorescence profiles contribute to the overall spectrum. However, due to the overlap of the fluorescent profiles of the NV^0 and NV^- , the contribution from each charge state is not immediately clear.

To distinguish between the spectral contribution of the two charge states we can train a machine-learning algorithm to identify the contribution of each NV charge state to a resultant spectrum. This problem can be addressed as a matrix factorization problem. The matrix to factorize is one where each wavelength corresponds to a column, and each spectrum in the data set corresponds to a row. The factors H and W correspond to the NV^0 and NV^- contributions, and their weightings for a specific spectrum respectively. In other words, we task the algorithm with finding two distinct features for which a linear combination can reconstruct each spectrum within the data set. With a large and diverse data set as provided through these experiments, this challenge is made tractable.

More specifically the matrix factorization will create the features, H , of dimension number of spectral contributions by number of wavelengths, and weights W of dimension number of spectra by number of spectral contributions. These two matrices will then multiply to reconstruct the measured spectra. The factorization task can be solved by a variety of methods such as principle component analysis or vector quantization but physical insight can narrow down our choices. There is no physical reason for us to record any negative intensities. Therefore, we can use non-negative matrix factorization which has been shown to be more effective for non-negative matrices [38, 39].

3.4.1 Non-negative Matrix Factorization

Non-negative matrix factorization (NMF) is a coordinate descent solver computed with the assumption that both factors, H and W , are positive matrices. An example of what the factorization would look like in the case of 2 components (e.g NV^0 and NV^- spectra) with n samples of data measured across m different wavelengths is given by,

$$\begin{bmatrix} W_{11} & W_{12} \\ W_{21} & W_{22} \\ \vdots & \vdots \\ W_{n1} & W_{n2} \end{bmatrix} \begin{bmatrix} H_{11} & H_{12} & \cdots & H_{1m} \\ H_{21} & H_{22} & \cdots & H_{2m} \\ \vdots & & \ddots & \vdots \\ H_{n1} & H_{n2} & \cdots & H_{nm} \end{bmatrix} = \begin{bmatrix} X_{11} & X_{12} & \cdots & X_{1m} \\ X_{21} & X_{22} & & X_{2m} \\ \vdots & & \ddots & \vdots \\ X_{n1} & X_{n2} & \cdots & X_{nm} \end{bmatrix}, \quad (3.4.1)$$

where X is the data given to the algorithm and H and W are uncovered through the factorization algorithm.

The task of computing this factorization, as an over-determined system, becomes a numerical task requiring iterative calculations and the minimization of a cost function. Python was chosen as there exist several packages which contain implementations of non-negative matrix factorization e.g [scikit-learn](#) and [Nimfa](#). Scikit-learn was selected as it had the flexibility to trial alternate factorization techniques if required. The scikit-learn package takes an initial guess (random or provided by the user) and iteratively calculates the objective (or cost) function as,

$$J = \frac{1}{2} \times \|\mathbf{X} - \mathbf{WH}\|_F^2, \quad (3.4.2)$$

where the subscript F is shorthand for the Frobenius norm. Other norms can be used for the

loss function as well as additions of regularization terms (norms of the individual components) to help prevent over-fitting. However, over-fitting is usually present if there are persistent random fluctuations in the training data that the algorithm attempts to fit to. Two things naturally prevent over-fitting in our case. First, there is a very large and diverse training data set which limits spurious additions from individual spectra. Second, each spectral measurement is smoothed and averaged reducing persistent noise sources in each measurement. The quality of this data, therefore, removes the need for regularization techniques which otherwise cause considerable increases in run times.

The python codebase to manage this task was created in two sections, a training section and an analysis section. The training section sought to process the spectra, taking in relative metadata for each spectrum, smoothing, cropping and removing unwanted features and then employing the NMF algorithm. Following the application, some basic validation steps are executed and the option to save the model is provided either in a text file or as a python class. The former provides flexibility between programs and versions, the latter provides ease of use (all metadata is saved as well). The analysis section provides various visualisations bespoke to the sensing modality creating contrast and sensitivity plots over the lifetime of the oxidation.

The NMF processing was split into two sections for two reasons. Firstly, there may be a distinction between the data required for training compared to analysis. One example is we may prefer to train the algorithm on the entire data set available but the analysis is usually conducted on diamond samples one at a time. The codebase was built with the utmost flexibility such that new samples can be incorporated into training algorithms or simply analysed using previously derived models. Secondly, the minimization algorithm can be initialized randomly and therefore an analysis might be bespoke to a specific random seed used to generate the model. Saving the model (along with any random seeds used to create it) ensures that reproducible analysis can be guaranteed.

3.4.2 Deconstructing 2keV implantations

We can start by applying the NMF algorithm to the 2keV sample discussed in [Chapter 2](#). By not supplying any guesses the NMF algorithm makes an interesting discovery of the relevant features. In Figure [3.4.1a](#) we can see that the components extracted are similar to the oil, coverslip and NV^0 spectra. We can assess the validity of these components by analysing the contribution to the overall spectrum as a function of time in Figure [3.4.1b](#). The NV^0 steadily increases throughout the oxidation whereas the oil and coverslip stay constant throughout the oxidation apart from at oxidation step 41. Comparing to the refocus issue mentioned in Figure [2.5.3c](#), the jump arose from an increase in fluorescence of the NV^0 and the oil (two adjacent components) as opposed to the coverslip. This is further supported by the analysis seen here where there is a small decrease in the coverslip contribution at step 41 and subsequent increase in the NV^0 and oil components of the fluorescence.

Attempts to fit any further features were met with weightings and components that weren't deemed physical for two reasons. First, the discovered components would unnecessarily decompose parts of the NV^0 spectrum. Second, the spectra derived also had jagged edges which seemed to be non-physical for the system under study. The lack of any alternate components arising from the NMF factorization of the 2keV sample also encourages the assertion that there is no NV^- present. That is to say, the sensing mechanism is due to the $\text{NV}^0 / \text{NV}^+$ transitions only.

The elucidation of the background spectra due to the oil, coverslip and other optical constants provides a feature that can be removed if sensing with a spectrometer. The fluorescence of these elements is negligible in sensing regimes of interest but will be important for generating factorizations of NV^- and NV^0 when the algorithm will favour absorbing the oil spectrum into the NV^0 or NV^- features.

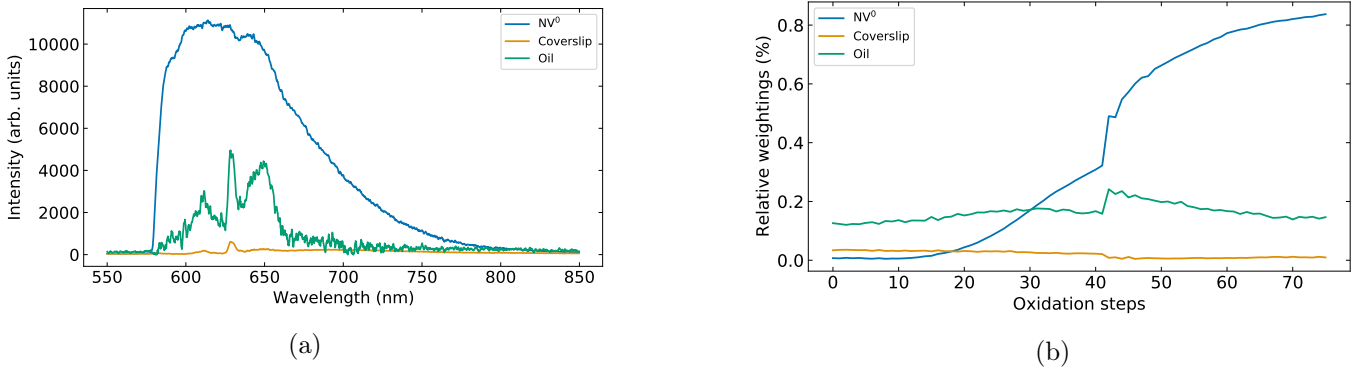


Figure 3.4.1: The deconstruction of the sample provided in chapter 2. Figure (a) provides the NV^0 , coverslip and oil components while (b) provides the magnitude of each weighting to reconstruct the each spectrum throughout the oxidation process.

The large data set derived from this method and initial success here suggests that NMF is a promising way to develop a characterisation of the NV^- and NV^0 fluorescence in samples with deeper implantations.

3.4.3 Deconstructing 4keV implantations

To understand NV charge state populations in the 4keV sample, and how they change, we can apply a new NMF algorithm to the 4keV oxidation data. Without any initial guesses, the NMF algorithm classifies something resembling the spectra of NV^0 and NV^- . However, the NMF algorithm struggles to classify the Raman line between the resulting spectral components as seen in Figure 3.4.2a. By subtracting a spectrum of the diamond Raman line from the spectra, we can provide data with only NV fluorescence to the NMF algorithm to get a better decomposition in Figure 3.4.2b.

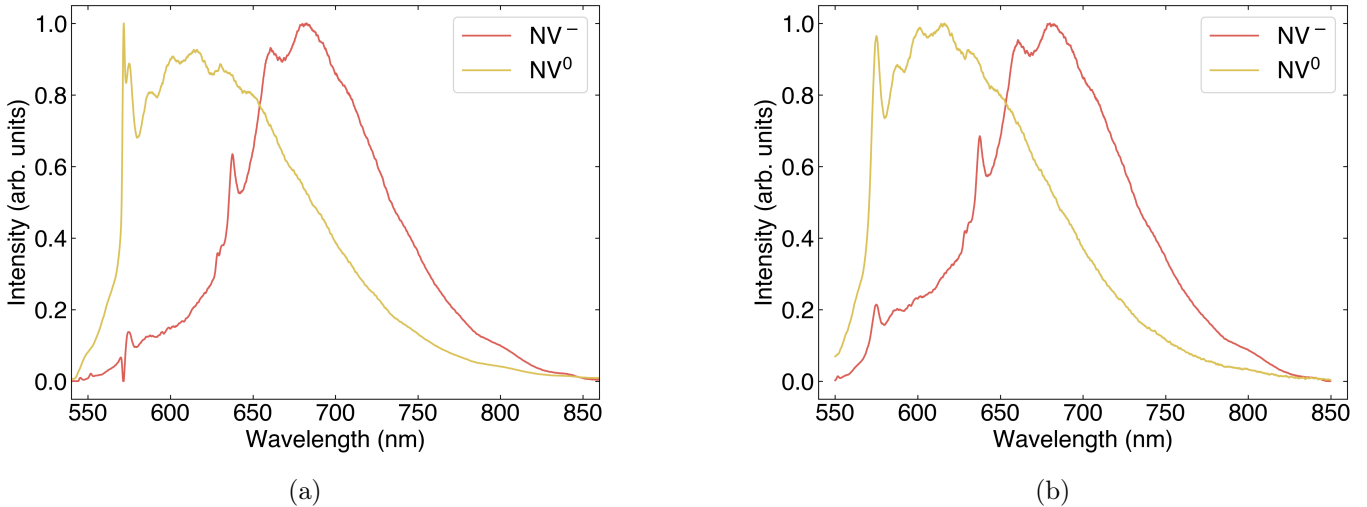


Figure 3.4.2: The deconstruction of the 4keV sample. (a) provides an initial fit which struggles to incorporate the Raman line at approximately 583nm.(b) shows the deconstruction after the Raman line is removed and smoothed over.

However, in the lower wavelengths ($\approx 575\text{-}625\text{nm}$) of the NV^- spectrum there seems to be a small NV^0 contribution. The result of this would therefore underestimate NV^0 populations and overestimate NV^- contributions. To affirm these deconstructions, and therefore estimates of charge state populations, we need to provide additional help to the NMF algorithm by providing some initial guesses for the components (H) and weights (W).

When placing an initial guess for the NMF algorithm we are required to provide both the weights and the spectral components. The spectral components can initially be estimated using the spectrum of hydrogenated and shallowly implanted samples which are dominated by NV^0 . Conversely, the NV^- component can be estimated by oxygenated and deeper implanted samples. These two sample spectra therefore constitute our initial guesses at the NV components, H , as given by Eq. 3.4.1.

However, the weightings are less consistent and depend on the implantation profile. For the 2keV sample explored previously there was close to 100% NV^+ in the original spectrum which gradually moved to NV^0 . In the 4keV sample, the dominant NV charge state concentration is NV^0 before oxidation. To make this quantitative, there is a diamond solving package [diamond-bandalyzer](#) (developed by Nikolai Dotschuk and Daniel J. McCloskey) which provides a theoretical relationship between the surface adsorbate density (the level of hydrogenation) and the NV charge state populations.

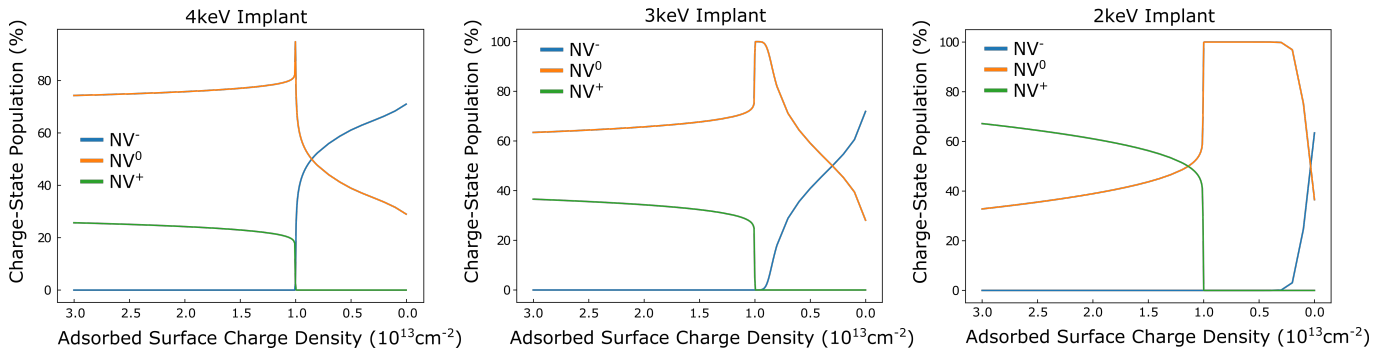


Figure 3.4.3: Theoretical calculations using the diamond bandalyzer program estimating the charge state populations as a function of adsorbed charge density (positive adsorbed charge density corresponds to higher hydrogen terminations).

By using the percentages provided in Figure 3.4.3 we can make an approximation as to the expected NV^- and NV^0 contributions to the spectra. When comparing the presence of NV^+ and NV^0 in Figure 3.4.3 to those observed in Section 3.4.2, we can approximate that the adsorbed surface charge density spans from 5×10^{14} to 1.5×10^{13} ions per cm^2 . We can therefore estimate the weightings, W , of the NV^0 and NV^- components over the oxidation. As initial guesses these estimations do not need to be exact. By combining the informed initial guess for the components, H , and weightings, W , we arrive at Figure 3.4.4.

One of the notable features, which is important for assessing the accuracy of these deconstructions, is the zero phonon line (ZPL). As described in the name, this is a bright peak in the fluorescence that marks the energy difference between the ground and first excited states of the NV centre meaning that no phonons are involved. The NV^0 has a ZPL at 575nm and the NV^- has a ZPL at 637nm. As can be seen in Figure 3.4.4 the ZPL correlates well with the deconstructions provided by the NMF algorithm. There is a small component of the NV^0 ZPL in the NV^- spectrum. However, in comparison to those provided in the literature shown in Figure 3.2.2, other techniques for discerning the NV^0 and NV^- profile also include this contribution most likely due to non-equilibrium photo-induced cycling between the NV^0 and NV^- states [40].

With this classification, we can now approximate the relative populations of different NV charge states in a sample. By understanding the relative populations of NV charge states we can understand why the implantation discussed here did not prove fruitful for dual charge state sensing. Furthermore, we can provide suggestions of NV charge state concentrations that will be appropriate for a dual charge state sensor.

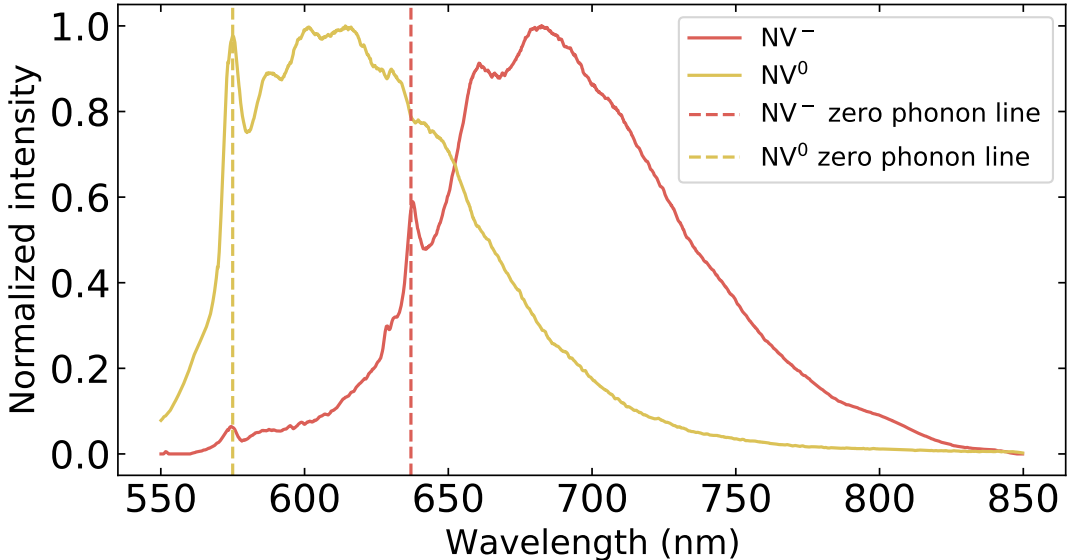


Figure 3.4.4: The NV^0 and NV^- components extracted from the non-negative matrix factorization by providing component guesses with independent components. The dotted line represent the zero phonon line, where an increase in fluorescence is expected, for the fluorescence of the two charge states.

3.4.4 Estimating NV charge states using fluorescent deconstructions

This section uses the fluorescence recorded throughout the oxidation procedure to estimate the change in charge state populations compared with a changing surface termination. By developing an assessment of these charge state populations we may be able to predict what range of NV populations will be favourable for dual charge state sensing applications in future.

To begin we require a baseline for understanding the NV population. In the most oxygenated state of the diamond, a majority of the NV centres will be in the NV^0 or NV^- state meaning that we can assume zero NV^+ . As can be seen in the band bending diagrams Figure 1.5.2 this would mean that all the NV centres are deeper than a certain depth within the diamond such that no NVs are in the NV^+ state. This cannot be guaranteed but, as can be seen by the domination of the NV^- in the final spectrum in Figure 3.4.5, this is not unreasonable.

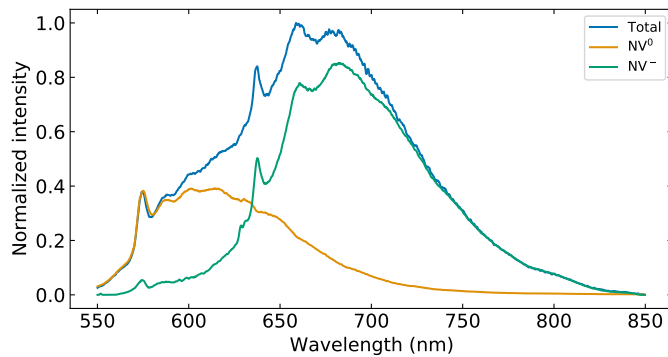


Figure 3.4.5: The NV^0 and NV^- components of the oxygen terminated sample

We can first decompose the oxygenated spectrum in Figure 3.4.5 into it's NV^0 and NV^- parts. We can then convert these charge state contributions into a NV charge state population by integrating and scaling by their excited state lifetimes. The excited state lifetime corresponds to the average time required for a single NV to relax to it's ground state after fluorescence has occurred.

The excited state lifetimes are different between the NV^0 and NV^- state and therefore needs to be considered when comparing NV^0 and NV^- fluorescence contributions. The excited state lifetimes provided by Hacquebarg et al. are 12ns for NV^0 and 18ns for NV^- [40]. Therefore, assuming zero NV^+ charge states we have a baseline fluorescence populations that can be expressed as,

$$\begin{aligned} \text{total fluorescence population} &= P_F = F_0\tau_0 + F_-\tau_- , \\ &= W_0^O \times \int H_0 d\lambda \times \tau_{\text{NV}^0} + W_-^O \times \int H_- d\lambda \times \tau_{\text{NV}^-} , \end{aligned} \quad (3.4.3)$$

where the subscripts denote the NV^0 ($= 0$) and NV^- ($= -$) contributions, while H , W^O and τ represent the NV components, the corresponding NV component weighting (for the oxygenated case), and the excited state lifetimes respectively. The NV^0 and NV^- populations can therefore be calculated as the ratio of the NV charge state fluorescence to the baseline fluorescence population defined in Eq. 3.4.3,

$$\rho_{\text{NV}^0} = \frac{W_0^{(i)} \times \int H_0 d\lambda \times \tau_{\text{NV}^0}}{P_F} \quad \text{and} \quad \rho_{\text{NV}^-} = \frac{W_-^{(i)} \times \int H_- d\lambda \times \tau_{\text{NV}^-}}{P_F} , \quad (3.4.4)$$

where ρ gives the percentage populations of the charge states and the superscript (i) is an index corresponding to the weighting for a specific spectrum in the data set. As these are all relative populations we can infer the NV^+ population as the remaining population using,

$$\rho_{\text{NV}^+} = 100\% - \rho_{\text{NV}^0} - \rho_{\text{NV}^-} . \quad (3.4.5)$$

By calculating these fluorescence populations we can derive a relative NV population as shown in Figure 3.4.6

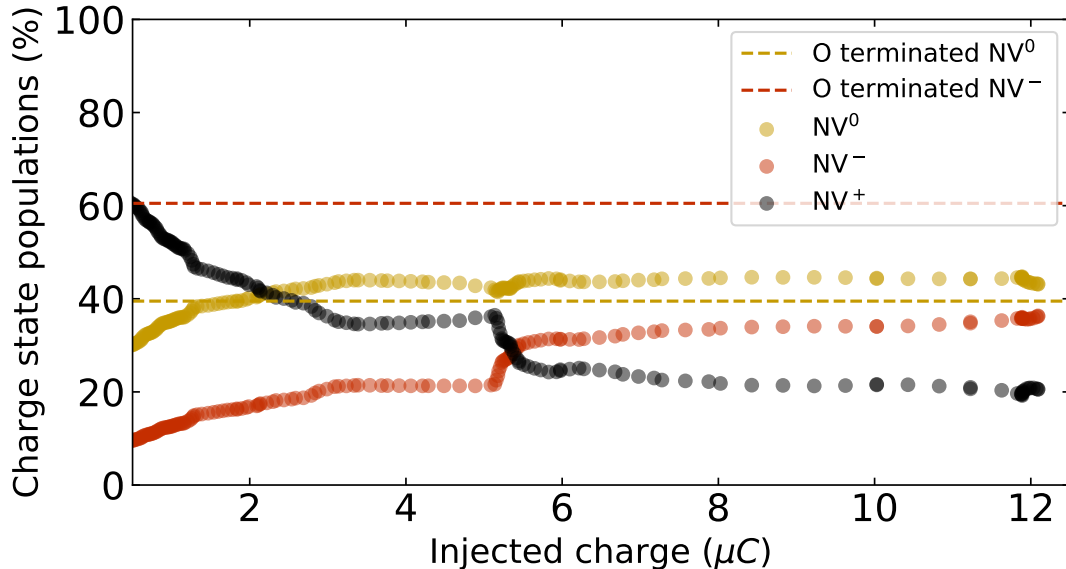


Figure 3.4.6: The relative populations NV^0 and NV^- throughout the oxidation procedure as calculated by the deconstructed fluorescence (calculated using Eq. 3.4.4 and Eq. 3.4.5).

Figure 3.4.6 shows that the NV^- and NV^0 populations never meet in a regime favourable for facilitating transitions between the NV^- and NV^0 . In comparison to Figure 3.4.3 the sample reflects an implantation profile more closely resembling something between a 3keV or 2keV implant. The discrepancy between expected fluorescence properties of a 4keV and those displayed here is most likely

due to unwanted etching in the hydrogenation process. There are still unpredictable components in the fabrication of these diamond voltage sensors and unfortunately etching can still occur bringing NVs closer to the surface.

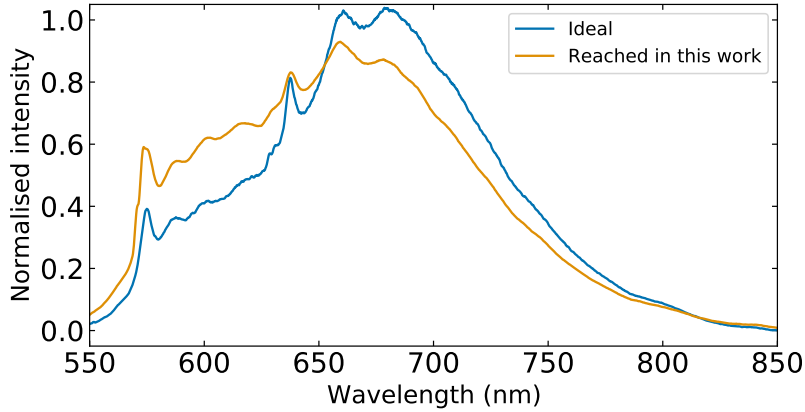


Figure 3.4.7: The "ideal" mix of NV^0 and NV^- states as suggested by Karaveli et al. of 25% and 75% respectively compared to the fluorescence mix reached in this work. [11]

Compared to Karaveli [11] which suggests a 75% to 25% split between NV^- and NV^0 respectively the populations attained here are not sufficient for sensing reaching a maximum of 38% NV^- and 42% NV^0 . We can compare the proposed 75%/25% fit to that achieved here in Figure 3.4.7. Although the optimal spectrum is not achieved within this work we can use the ideal spectrum in future cases to evaluate the candidacy of samples for dual charge state or single charge state sensing.

In future testing, we can recommend that samples of 4keV implantation depth or further are explored for dual charge state sensing but great care needs to be made not to etch the surface. With the results of the following analysis, we can now evaluate a samples suitability for dual charge state sensing via this decomposition analysis and requiring that samples need NV^0 populations to be less than 40% and NV^- populations to be greater than 60% prior to hydrogenation.

Throughout this chapter, we took on the challenge of forming a dual charge state sensor. Here the alteration of the surface chemical species became an invaluable tool for providing a decomposition of the NV^0 and NV^- fluorescence. This decomposition will help to provide a new record for predicting the proximity of NVs to the surface of the diamond and therefore classify NV implantations in their candidacy as a single or dual charge state sensor.

Chapter 4

Concluding remarks and next steps

This thesis demonstrates the capability of electrochemical methods to tune a diamond voltage sensor to a maximal sensitivity. The procedure was demonstrated with two sensing modalities: a single charge state sensor ideal for voltage microscopy and a dual charge state sensor for bulk measurements in high noise environments.

First, the electrochemical method was shown to increase the sensitivity of a diamond voltage sensor to levels 30 times its pre- and post-tuning state. Moreover, the optimum contrast is a factor of 20 times better than those currently reported in literature for single crystal voltage sensing [1]. The electrochemical procedure achieved bespoke surface mixtures and provided a significant leap forward for realising a diamond voltage sensor. The results of this optimisation not only demonstrated electrochemical tuning as a valid optimisation parameter but also launched the diamond voltage sensor's potential to compete with existing voltage sensing technologies. The results of this study contributed to a demonstration of the diamond voltage imaging microscope which has been accepted for publication in *Nature Photonics*.

With the success provided by Chapter 2, a more ambitious goal was sought to optimise a dual charge state sensor. The alternate sensing modality may be more robust to noise pushing the boundaries of sensitivity for large scale electric fields such as very low-frequency electromagnetic radiation. However, the challenge was considerable due to the significant spectral overlap of the two charge state fluorescence profiles. Contrasts and voltage sensitivity regimes relevant for sensing applications were not realised for this sensing modality due to the NV centres being too close to the surface in the sample studied. Yet, the data provided methods to characterise diamond voltage sensors for microscopy or potentiometry by extracting population estimates from fluorescent recordings. These were developed using fluorescence feature deconstruction. The characterisation reports on relative NV populations and provides the groundwork for realising dual charge state sensors in future work.

There are three further explorations of interest enabled by the work demonstrated here. First, the immediate follow up from this work is to explore the electrochemical oxidation of a diamond with deeper NVs as a dual charge state sensing candidate. The work outlined here provides a promising first step towards understanding the required depth and therefore equilibrium populations of NV charge states. This work has already been started by the author but unfortunately, time constraints did not allow for the processing and analysis of this work to be completed and included in this thesis. The experiment also trialled using three spectral ranges for sensing. Fluorescence through an NV^0 and NV^- bandpass filter, as well as the total fluorescence, was collected during this trial alongside intermittent spectrometer measurements. In the future procurement of multiple fluorescent detectors (e.g cameras or photodiodes) would also be required to read the different fluorescent signals simultaneously. Exploratory work was trialled using photodiodes however the count rate was too low for sensing applications suggesting that an avalanche photodiode would be more suitable for the dual charge state sensing application.

Secondly, although tuning was explored for both sensing modalities and shown to span different

regimes, the control of the electric characteristics needs to be explored further. There was again work done on this front by the author to collect current-voltage characteristics with the Keithley source meter however analysis showed that short circuit was present in the system hindering conclusive results. Improving the understanding of what voltage is required for a Faradaic current as well as how this voltage evolves would provide even finer control over the optimisation procedure. By modelling characteristics such as shunting current and capacitive charging effects one could also find numerical values for other important constituents of the device. Constituents such as the electrolytic double layer capacitance, quantum capacitance and any shunting current effects from the contacts will give greater insight into the charge dynamics in sensing applications. To improve the diamond device above existing voltage sensing technologies, optimisation parameters are not only important to identify but also capabilities for measuring these parameters become paramount for finer tuning to take place.

Finally, hydrogenation techniques are well established and repeatable providing a consistent initial state to work from. However, an in-solution process for hydrogenating the surface to reverse the above treatment would demonstrate an even greater control with respect to surface tuning. The advent of an in solution hydrogenation technique would allow *in situ* hydrogenation in cases where optimal contrasts were surpassed. The electrochemical hydrogenation has been demonstrated with BDD micro-crystalline diamonds [26]. However, there have been no demonstrations for single-crystal diamonds. Daniel McCloskey and the author have made attempts to reduce hydrogen onto a partially hydrogenated diamond using UV illumination while applying reverse potentials in an acidic solution. But long term hydrogenation remains elusive. The realisation of this as a technique would provide the utmost control of the surface termination allowing the electrochemical method to be bidirectional.

The work outlined here provides a clear method for optimising diamond voltage sensors by modifying the surface termination. Not only that but this work demonstrates the best contrast provided by this sensing modality currently seen in the literature with a 20 fold increase in reported contrasts in single crystal voltage sensors from 0.02% [1] to 0.45% in this work. Moreover, the work outlined here makes ground towards realising a dual charge state sensor built on overcoming noise floors by providing anti-correlated fluorescent signals. The third chapter provides a novel method for estimating charge state populations using a machine learning algorithm applied to fluorescent spectra. The methods demonstrated here provide tools for evaluating and tuning diamond voltage sensors for future applications from measuring neural networks to twitching frog legs.

Bibliography

- [1] Grotz, B., et al. *Nature Communications* **3**(1), 729 March (2012).
- [2] Kittel, C. and McEuen, P. *Introduction to Solid State Physics*. John Wiley & Sons, June (2018).
- [3] Pleskov, Y. V., et al. *Russian Journal of Electrochemistry* **52**(1), 1–6 January (2016).
- [4] Gandini, D., et al. *Journal of Applied Electrochemistry* **30**(12), 1345–1350 December (2000).
- [5] Hébert, C., et al. *Faraday Discussions* **172**(0), 47–59 November (2014).
- [6] Achard, J., et al. *Diamond and Related Materials* **20**(2), 145–152 February (2011).
- [7] Ngambou, M. W. N., et al. *Diamond and Related Materials* **123**, 108884 March (2022).
- [8] Dresselhaus, M. S. and Kalish, R. *Ion Implantation in Diamond, Graphite and Related Materials*. Springer Science & Business Media, March (2013).
- [9] Rondin, L., et al. *Reports on Progress in Physics* **77**(5), 056503 May (2014). Publisher: IOP Publishing.
- [10] Simpson, D. A., et al. *ACS Nano* **11**(12), 12077–12086 December (2017).
- [11] Karaveli, S., et al. *Proceedings of the National Academy of Sciences* **113**(15), 3938–3943 April (2016).
- [12] Hong, S., et al. *MRS Bulletin* **38**(2), 155–161 February (2013). Publisher: Cambridge University Press.
- [13] Radishev, D., et al. *Journal of Luminescence* **239**, 118404 November (2021).
- [14] Dhomkar, S., et al. *Nano Letters* **18**(6), 4046–4052 June (2018).
- [15] Hauf, M. V., et al. *Physical Review B* **83**(8), 081304 February (2011).
- [16] Hanlon, L., et al. *Neurophotonics* **7**(3), 035002 August (2020). Publisher: SPIE.
- [17] Alba, G., et al. *Nanomaterials* **10**(6), 1193 June (2020).
- [18] Navas, J., et al. *Applied Surface Science* **433**, 408–418 March (2018).
- [19] Pehrsson, P. E. and Mercer, T. W. *Surface Science* **460**(1), 74–90 July (2000).
- [20] Rutter, M. J. and Robertson, J. *Computational Materials Science* **10**(1), 330–333 February (1998).
- [21] Sque, S. J., et al. *Physical Review B* **73**(8), 085313 February (2006).
- [22] Landstrass, M. I. and Ravi, K. V. *Applied Physics Letters* **55**(14), 1391–1393 October (1989).
- [23] Maier, F., et al. *Physical Review Letters* **85**(16), 3472–3475 October (2000).
- [24] Riedel, M., et al. *Physical Review B* **69**(12), 125338 March (2004).
- [25] Gaisinskaya, A., et al. *Diamond and Related Materials* **18**(12), 1466–1473 December (2009).
- [26] Hoffmann, R., et al. *Applied Physics Letters* **97**(5), 052103 August (2010).
- [27] Pate, B. B. *Surface Science* **165**(1), 83–142 January (1986).
- [28] Hoffmann, R., et al. *Langmuir* **28**(1), 47–50 January (2012). Publisher: American Chemical Society.
- [29] Chaplin, B. P., et al. *Electrochimica Acta* **89**, 122–131 February (2013).
- [30] Carter, B. C. and Bean, B. P. *Neuron* **64**(6), 898–909 December (2009).
- [31] McCloskey, D. J., et al. *ACS Applied Materials & Interfaces* **12**(11), 13421–13427 March (2020).
- [32] Xing, K., et al. *Applied Physics Letters* **116**(11), 111601 March (2020).
- [33] Dankerl, M., et al. *Physical Review Letters* **106**(19), 196103 May (2011).
- [34] Luryi, S. *Applied Physics Letters* **52**(6), 501–503 February (1988).
- [35] Ragheb, T. and Geddes, L. A. *Annals of Biomedical Engineering* **19**(2), 151–163 March (1991).
- [36] Aslam, N., et al. *New Journal of Physics* **15**(1), 013064 January (2013).
- [37] Chakraborty, T., et al. *Physical Review Applied* **17**(2), 024046 February (2022).
- [38] Paatero, P. and Tapper, U. *Environmetrics* **5**(2), 111–126 (1994).
- [39] Lee, D. D. and Seung, H. S. *Nature* **401**(6755), 788–791 October (1999).
- [40] Hacquebard, L. and Childress, L. *Physical Review A* **97**(6), 063408 June (2018).